



**NAVAL  
POSTGRADUATE  
SCHOOL**

**MONTEREY, CALIFORNIA**

**THESIS**

**EVALUATION OF ADCP WAVE MEASUREMENTS**

by

Jeremy David Boyd

December 2006

Thesis Advisor: Thomas H.C. Herbers  
Second Reader: Edward B. Thornton

**Approved for public release; distribution unlimited**

THIS PAGE INTENTIONALLY LEFT BLANK

<b>REPORT DOCUMENTATION PAGE</b>		Form Approved OMB No. 0704-0188	
Public reporting burden for this collection of information is estimated to average 1 hour per response, including the time for reviewing instruction, searching existing data sources, gathering and maintaining the data needed, and completing and reviewing the collection of information. Send comments regarding this burden estimate or any other aspect of this collection of information, including suggestions for reducing this burden, to Washington headquarters Services, Directorate for Information Operations and Reports, 1215 Jefferson Davis Highway, Suite 1204, Arlington, VA 22202-4302, and to the Office of Management and Budget, Paperwork Reduction Project (0704-0188) Washington DC 20503.			
<b>1. AGENCY USE ONLY (Leave blank)</b>	<b>2. REPORT DATE</b> December 2006	<b>3. REPORT TYPE AND DATES COVERED</b> Master's Thesis	
<b>4. TITLE AND SUBTITLE</b> Evaluation of ADCP Wave Measurements		<b>5. FUNDING NUMBERS</b>	
<b>6. AUTHOR</b> Jeremy David Boyd		<b>8. PERFORMING ORGANIZATION REPORT NUMBER</b>	
<b>7. PERFORMING ORGANIZATION NAME(S) AND ADDRESS(ES)</b> Naval Postgraduate School Monterey, CA 93943-5000		<b>10. SPONSORING/MONITORING AGENCY REPORT NUMBER</b>	
<b>9. SPONSORING /MONITORING AGENCY NAME(S) AND ADDRESS(ES)</b> N/A		<b>11. SUPPLEMENTARY NOTES</b> The views expressed in this thesis are those of the author and do not reflect the official policy or position of the Department of Defense or the U.S. Government.	
<b>12a. DISTRIBUTION / AVAILABILITY STATEMENT</b> Approved for public release; distribution is unlimited		<b>12b. DISTRIBUTION CODE</b>	
<b>13. ABSTRACT (maximum 200 words)</b> Nearshore wave information is important to a variety of United States Navy operations in the littorals, including mine warfare, amphibious operations, small boat operations and special forces insertions. The objective of this thesis is to evaluate the accuracy of Teledyne RDI Acoustic Doppler Current Profilers (ADCP), in measuring wave height and direction spectra, so that the military can use these for routine wave measurements nearshore. This study uses ADCP data collected in 25 and 45 m depths during the fall 2003 Nearshore Canyon Experiment (NCEX) off La Jolla, California. Data were first corrected for dropouts. Next the data quality was verified through a consistency check on the redundant velocity measurements of opposing beams, an evaluation of high frequency spectral noise levels, and a comparison of velocity and pressure measurements using linear wave theory. Finally wave height and direction spectra estimated from the ADCP data were compared to data from a directional wave buoy. The analysis revealed that the ADCP data can suffer from low signal to noise ratios in benign conditions and deeper water. Whereas the wave height estimates are sensitive to these errors, the wave direction estimates are surprisingly robust.			
<b>14. SUBJECT TERMS</b> Undersea Warfare, Littoral Wave Measurements, ADCP, Ocean Waves		<b>15. NUMBER OF PAGES</b> 71	<b>16. PRICE CODE</b>
<b>17. SECURITY CLASSIFICATION OF REPORT</b> Unclassified	<b>18. SECURITY CLASSIFICATION OF THIS PAGE</b> Unclassified	<b>19. SECURITY CLASSIFICATION OF ABSTRACT</b> Unclassified	<b>20. LIMITATION OF ABSTRACT</b> UL

THIS PAGE INTENTIONALLY LEFT BLANK

Approved for public release; distribution unlimited

**EVALUATION OF ADCP WAVE MEASUREMENTS**

Jeremy David Boyd  
Lieutenant, United States Navy  
B.G.S., University of Kansas, 1999

Submitted in partial fulfillment of the  
requirements for the degree of

**MASTER OF SCIENCE IN PHYSICAL OCEANOGRAPHY**

from the

**NAVAL POSTGRADUATE SCHOOL  
December 2006**

Author: Jeremy David Boyd

Approved by: Thomas H.C. Herbers  
Thesis Advisor

Edward B. Thornton  
Second Reader

Mary L. Batteen  
Chairman, Department of Oceanography

Donald P. Brutzman  
Chair, Undersea Warfare

THIS PAGE INTENTIONALLY LEFT BLANK

## ABSTRACT

Nearshore wave information is important to a variety of United States Navy operations in the littorals, including mine warfare, amphibious operations, small boat operations and special forces insertions. The objective of this thesis is to evaluate the accuracy of Teledyne RDI Acoustic Doppler Current Profilers (ADCP), in measuring wave height and direction spectra, so that the military can use these for routine wave measurements nearshore. This study uses ADCP data collected in 25 and 45 m depths during the fall 2003 Nearshore Canyon Experiment (NCEX) off La Jolla, California. Data were first corrected for dropouts. Next the data quality was verified through a consistency check on the redundant velocity measurements of opposing beams, an evaluation of high frequency spectral noise levels, and a comparison of velocity and pressure measurements using linear wave theory. Finally wave height and direction spectra estimated from the ADCP data were compared to data from a directional wave buoy. The analysis revealed that the ADCP data can suffer from low signal to noise ratios in benign conditions and deeper water. Whereas the wave height estimates are sensitive to these errors, the wave direction estimates are surprisingly robust.

THIS PAGE INTENTIONALLY LEFT BLANK

## TABLE OF CONTENTS

I.	INTRODUCTION .....	1
A.	MOTIVATION .....	1
B.	ROUTINE WAVE MEASUREMENT SYSTEMS .....	3
C.	THE ACOUSTIC DOPPLER CURRENT PROFILER (ADCP) .....	4
D.	OBJECTIVE AND SCOPE .....	6
II.	EXPERIMENT .....	7
A.	FIELD SITE .....	7
1.	Teledyne Workhorse Sentinel ADCP .....	7
2.	Mooring Configuration .....	8
3.	Velocity Cells .....	10
III.	DATA ANALYSIS .....	13
A.	QUALITY CONTROL OF DATA .....	13
1.	Site 18 Data Quality Control .....	13
2.	Site 19 Data Quality Control .....	14
B.	BEAM COMPARISONS .....	15
C.	NOISE FLOOR .....	16
IV.	VERIFICATION LINEAR TRANSFER FUNCTION .....	23
A.	PRESSURE-VELOCITY TRANSFER FUNCTION .....	23
B.	SPECTRAL COMPARISONS .....	23
C.	VARIANCE COMPARISONS .....	25
V.	DIRECTIONAL WAVE SPECTRA .....	33
A.	ESTIMATION TECHNIQUE .....	33
1.	The Frequency-Directional Wave Spectrum .....	33
2.	Transfer Functions for ADCP Velocity Measurements .....	34
3.	Estimate of the Frequency Spectrum .....	35
4.	Estimate of the Directional Distribution .....	36
B.	CASE STUDIES .....	39
1.	October 30 <sup>th</sup> 1800 PST .....	39
2.	November 17 <sup>th</sup> 0000 PST .....	40
3.	November 22 <sup>nd</sup> 1800 PST .....	40
VI.	CONCLUSIONS .....	47
	LIST OF REFERENCES .....	51
	INITIAL DISTRIBUTION LIST .....	53

THIS PAGE INTENTIONALLY LEFT BLANK

## LIST OF FIGURES

Figure 1.	NCEX array plan. Directional Waverider buoys are shown as yellow triangles, bottom pressure recorders are red squares, PUV sensors are white circles, and current profilers are brown diamonds. The inset shows the three instruments used in this study. <a href="http://www.oc.nps.navy.mil/wavelab/ncex.html">http://www.oc.nps.navy.mil/wavelab/ncex.html</a> , Retrieved October 2006.....8	8
Figure 2.	Teledyne Workhorse Sentinel ADCP (upper photo) mounted on Sea-Spider prior to deployment (lower photo). Mounted below the instrument is an extra battery pack. Attached to the front side of the Sea-Spider is the acoustic release assembly with a recovery buoy. (Upper photo from <a href="http://www.rdinstruments.com/sen.html">http://www.rdinstruments.com/sen.html</a> ), Retrieved October 2006.....11	11
Figure 3.	ADCP schematic detailing beams and velocity cells. $d_p$ is the height of the transducer and pressure sensor above the bed (0.6m). $d_m$ is the height of cell $m$ highlighted in blue, $h$ is the total depth of water, $m$ is the velocity cell index, and $\alpha$ is the angle of the beams relative to vertical (20 degrees).....12	12
Figure 4.	Example wave burst time series (units mm/s) from site 18. From top to bottom: (a) Clean data. (b) A typical burst with some dropouts. (c) The same burst after dropouts were corrected. (d) A burst of low quality data that could not be corrected.....15	15
Figure 5.	Site 18 velocity variances (units (m/s) <sup>2</sup> ), from opposing beams (a) 1, 2 and (b) 3, 4. Results from all six bins are shown, from near the surface (top) to the near sea floor (bottom)....18	18
Figure 6.	Site 19 velocity variances (units (m/s) <sup>2</sup> ). (Same format as Figure 5).....19	19
Figure 7.	Site 18 high frequency velocity variances (units (mm/s) <sup>2</sup> ) of all four beams. Uncorrected data is shown in (a) and corrected data in (b). The top panels show the uppermost bin, the bottom panels the lowest bin.....20	20
Figure 8.	Site 19 high frequency velocity variances (units (mm/s) <sup>2</sup> ). (Same format as Figure 7).....21	21

Figure 9.	Comparison of bottom pressure spectrum at site 18 estimated from ADCP velocity measurements at 6 depth cells and the directly measured pressure spectrum.....	26
Figure 10.	Comparison of bottom pressure spectrum at site 18 predicted from ADCP velocity measurements with directly measured pressure. The lower panel shows time series from one of the cells (5) with many spikes that degrade the spectrum estimate.....	27
Figure 11.	Comparison of bottom pressure spectrum at site 18 predicted from ADCP velocity measurements with the directly measured pressure spectrum. Bottom panel: Time series of cell 11 that show large shifts in beams 1 and 4.....	28
Figure 12.	Comparison of bottom pressure spectrum at site 19 predicted from ADCP velocity measurements and directly measured pressure. (Same format as Figure 9).....	29
Figure 13.	Comparison of ADCP-derived bottom pressure variances at site 18 with directly measured pressure variance. The top panel shows estimates for all six depth cells. The bottom panel shows the ratio between predicted and measured pressure variance.....	30
Figure 14.	Comparison of ADCP-derived bottom pressure variances at site 19 with directly measured pressure variance. (Same format as Figure 13)...	31
Figure 15.	Power cosine model showing the directional distribution of wave energy where $\sigma$ is the directional spread (i.e., half-width of the distribution) and the mean wave direction is denoted by $\bar{\theta}$ .....	38
Figure 16.	October 2003 wave statistics compendium plot taken from the Coastal Data Information Program (CDIP)website. The location of the buoy (deployed as part of the NCEX experiment) is shown in Figure 1. From top to bottom: significant wave height, peak period, and dominant wave direction. Highlighted in red is the first case study October 30 <sup>th</sup> .....	42
Figure 17.	November 2003 wave statistics (same format as Figure 16).....	43
Figure 18.	Case I ADCP and wave buoy comparisons. From top to bottom are shown the surface height spectrum, the mean direction for site 18 and	

mean direction for site 19. The dashed lines in the lower two panels indicate the mean direction  $\bar{\theta} \pm$  the directional spread  $\sigma$ .....44

Figure 19. Case II ADCP and wave buoy comparisons (same format as Figure 18).....45

Figure 20. Case III ADCP and wave buoy comparisons (same format as Figure 18).....46

THIS PAGE INTENTIONALLY LEFT BLANK

## LIST OF TABLES

Table 1.	Configuration and data collection details of ADCPs at sites 18 and 19.....	9
----------	----------------------------------------------------------------------------	---

THIS PAGE INTENTIONALLY LEFT BLANK

## ACKNOWLEDGMENTS

The field data were collected by T.H.C. Herbers, W.C. O'Reilly and S. Lentz with funding provided by the National Science Foundation and the Office of Naval Research. Dr. Steve Lentz provided the two ADCP instruments for this study.

I owe much to the professionalism and dedication of Professor T.H.C. Herbers and Mr. Paul Jessen. Without their support this research would not have been possible. I am forever grateful for their kindness and above all their patience in guiding me through this research.

I would also like to thank Professor Ed Thornton for agreeing to be my second reader and Dr. Tim Janssen for his encouragement along the latter part of this journey.

I want to thank my family, particularly my wife Elizabeth, who has fully supported me throughout this journey.

THIS PAGE INTENTIONALLY LEFT BLANK

## I. INTRODUCTION

### A. MOTIVATION

Since the end of the Cold War and the start of the Global War on Terrorism the United States Navy has found itself operating in the littoral regions of the World. From amphibious operations, mine-hunting, and Special Forces insertions, the importance of understanding the nearshore battlespace environment is important for current and future military operations. Unknown conditions in the nearshore environment can have a negative impact on military operations. The dynamic conditions of the nearshore environment, in particular waves, currents, and changes in seabed morphology must be accurately understood if littoral Navy operations are to be carried out successfully.

Ocean surface waves are generated by wind forces on the ocean surface and can travel freely across ocean basins with very little loss in energy. As these waves approach and collide with the shore, the energy in the waves is dissipated in the surf zone. The wave energy can be distributed relatively uniformly along the beach as in the case of gently sloping shores or concentrated as in the case of headlands or points. Even on simple coastlines wave conditions are often highly variable owing to refraction and diffraction by topography. In shallow nearshore waters, waves drive alongshore currents, undertow, and rip currents, often creating a challenging environment for small boats.

Traditionally, wave conditions have been characterized by a few parameters, such as a representative wave height,

period and propagation direction. However, the sea state is often complex with multiple wave systems present. For example, a locally generated wind sea may be accompanied by swell from a distant storm. In the nearshore environment the presence of an underwater shoal can create a complex wave field with crossing seas.

A more detailed description of the sea state is given by the frequency directional spectrum  $E(f,\theta)$  that defines the distribution of wave energy as a function of frequency  $f$  and direction  $\theta$ .

The confused nature of multimodal seas can affect ship maneuvering, response, and even personnel onboard. Accurate predictions or measurements of the wave spectrum are needed to predict ship pitch, roll, and heave motions that can place a ship's stability in jeopardy (Beal, 1991). Wave conditions can also change rapidly and this can impact all aspects of the littoral environment. Bathymetry readings taken days earlier may have changed due to sediment transport and wave energy concentrations that can change just as rapidly interrupting amphibious or minesweep operations.

The United States Navy has sophisticated models, such as WaveWatch III and Simulating WAVes Nearshore (SWAN), that predict wave parameters and spectra on a global and regional scale. However, model predictions contain considerable uncertainty, especially during benign sea conditions when small boat and nearshore Navy operations are usually conducted. These models are only as good as the winds that drive them and accuracy is better under strong wind-forcing conditions than in light wind and swell

conditions. Instead of relying solely on models, an effective wave prediction system should include some direct wave measurements that can be assimilated in the model to improve accuracy of the forecast or nowcast.

#### **B. ROUTINE WAVE MEASUREMENT SYSTEMS**

There are many instruments that can be used to measure waves in littoral regions (Allender et al., 1989). Some have inherent advantages for operating in this energetic environment. The most commonly used instruments are point measurement systems, such as surface following buoys (Longuet-Higgins et al., 1963) and bottom-mounted pressure sensor-current meter (PUV) systems (Bowden and White, 1966).

There are many different types of wave buoys. The widely used Datawell Directional Waverider uses three component acceleration sensors together with tilt sensors and a compass, to measure the sea surface motion in three dimensions. One acceleration sensor measures the vertical displacements (yielding wave height and period information) and the other two sensors measure the horizontal buoy displacements (yielding wave direction). Another type of buoy known as a "pitch and roll buoy" (Longuet-Higgins et al., 1963) measures tilt angles or pitch and roll to calculate wave direction. Newer buoys use global positioning systems (GPS) to obtain wave height and direction measurements. Wave buoys are reliable and able to withstand heavy seas. However, wave buoys are heavy, costly and cannot be deployed clandestinely from remote vehicles. Furthermore, their mooring designs are not suitable for very shallow water (< 15m) deployments.

In shallow water PUV systems are often used to collect routine wave measurements (Thornton and Krapohl, 1974). Different types of velocity sensors have been used in PUV systems, including electro-magnetic (EM) current meters (Guza et al., 1988), acoustic Doppler velocimeters (ADV) (Herbers et al., 1991) and acoustic travel time (ATT) sensors. ADV sensors have largely replaced EM sensors in PUV systems due to their higher accuracy. The ADV sensor measures the Doppler shift in sound scattered from small particles that are advected with the wave orbital motion. Unlike the EM and ATT, the ADV is nonintrusive, measuring the undisturbed flow away from the probe. However, the ADV sensor performance can suffer from weak returns if there are few scatterers present in the water column.

ATT sensors have one advantage in that they can be used in clear water. ATT sensors measure the travel time of sound between a pair of probes and thus do not depend on the back scatter from particles in the water column. Disadvantages of ATT sensors are that they can be affected by air bubbles, biofouling, and are somewhat intrusive in the flow field.

### **C. THE ACOUSTIC DOPPLER CURRENT PROFILER (ADCP)**

In addition to the widely used surface buoys and PUV systems, Acoustic Doppler Current Profilers (ADCPs) have been adopted recently for use as a directional wave gauge. ADCPs are among the most widely used instruments in oceanographic research and are a cost effective way to measure profiles of water velocities and directional wave information (Pinkel and Smith 1987; Krogstad et al.; 1988; Smith, 1989).

The ADCP uses the basic principle of Doppler shifting to measure the orbital velocities of waves. The ADCP is normally bottom mounted and upward facing, and the instrument ensonifies the entire water column along four beams. The sound pulses are backscattered from small inorganic and organic particles that are advected by the wave motion causing a Doppler shift in the returned sound. The backscatter return is range-gated into a series of bins along the beams to surmise the velocity profile.

In addition to the wave orbital velocity measurements, the ADCP also measures the surface height through echo ranging (surface track) and bottom pressure with it's built in pressure sensor.

An important advantage of the ADCP is that it measures wave velocities at many locations as opposed to PUV systems that measure only at a single location. This array of velocity measurements potentially provides a more detailed description of directionality. This capability is important in situations with complex multimodal sea states that cannot be resolved with a PUV system (RD Instruments Wave Primer).

A disadvantage of the ADCP is that there must be scatterers present in the water column. ADCPs also can suffer from side-lobe interference that occurs when some of the energy from the sound pulse leaves the main path of the sound pulse and reflects from the sea bed or sea surface. This interference can overwhelm the scattered sound return from particles in the water column.

The ADCP is clearly a versatile instrument that shows great promise for operational use by the U.S. Navy. For

example, the ADCP could be mounted on an autonomous undersea vehicle (AUV) to stealthily gather information in hostile environments.

#### **D. OBJECTIVE AND SCOPE**

Using ADCP's for routine wave measurements is relatively new. The available literature on the ADCP wave measurements is sparse to date. In a previous study comparing the performance of ADCP derived wave spectra with other independent measurements, the manufacturer RDI concluded that a bottom-mounted upward-looking ADCP provides a robust means of determining wave height and direction in coastal-depth waters. The study also concluded that the directional spectra tend to be sharper than those from point measurements (Strong et al., 2000).

These and other comparisons show qualitative agreement, but questions remain about the basic accuracy of ADCP wave velocity measurements and its performance in a range of sea states. The main objective of this study is to understand the limitations of the ADCP and the basic accuracy of velocity measurements.

Chapter II describes the field site, data collection and the equipment used and its configuration. Chapter III reviews the data quality control procedures and analysis methods. In Chapter IV, the quality of velocity data is verified through comparisons with pressure data using linear theory transfer functions. In Chapter V, the ADCPs ability to measure wave directional spectra is evaluated through comparisons with a wave buoy. Finally the results are summarized in Chapter VI.

## **II. EXPERIMENT**

### **A. FIELD SITE**

The Nearshore Canyon Experiment (NCEX) was conducted between September and December 2003 near La Jolla, California. The field site is near two submarine canyons. The main La Jolla Canyon branches over in the steep and narrow Scripps Canyon that comes within 200 m of Blacks Beach and strongly affects the nearshore wave climate (Peak, 2004; Magne et al., 2006).

Large arrays of instruments were deployed to investigate the wave transformation across the canyons. These arrays include seven surface-following wave buoys, 17 bottom pressure recorders, 12 pressure-velocity sensors (PUV) and seven acoustic Doppler current profilers (ADCP) (Figure 1). The focus of this study will be on two ADCPs deployed at sites 18 and 19 (Figure 1) at the northern edge of the experiment site where the effects of the canyons are insignificant.

### **B. INSTRUMENTS AND DATA COLLECTION**

#### **1. Teledyne Workhorse Sentinel ADCP**

Sensors used were the Teledyne Workhorse Sentinel Acoustic Doppler Current Profiler (ADCP) with wave option (Figure 2). The Sentinel is a self-contained, 20 degree, four beam convex, ADCP. It employs a broadband signal processor and is capable of providing profile ranges from 1 to 165 meters at a depth of 200 m. It is capable of two Hz ping rates and can operate at 1200, 600, or 300 kHz.

The two ADCPs at sites 18 and 19 were configured at 600 kHz and table 1 provides the set up configuration. The data received from sites 18 and 19 were in the form of raw

velocity time-series from six selected cells for each of the four beams. The cells were selected to span the water column, excluding the near-bottom and near-surface bins that are contaminated by boundary effects. A 68-minute-long data burst consisting of 8192 samples at a 2 Hz sample rate was collected every three hours.

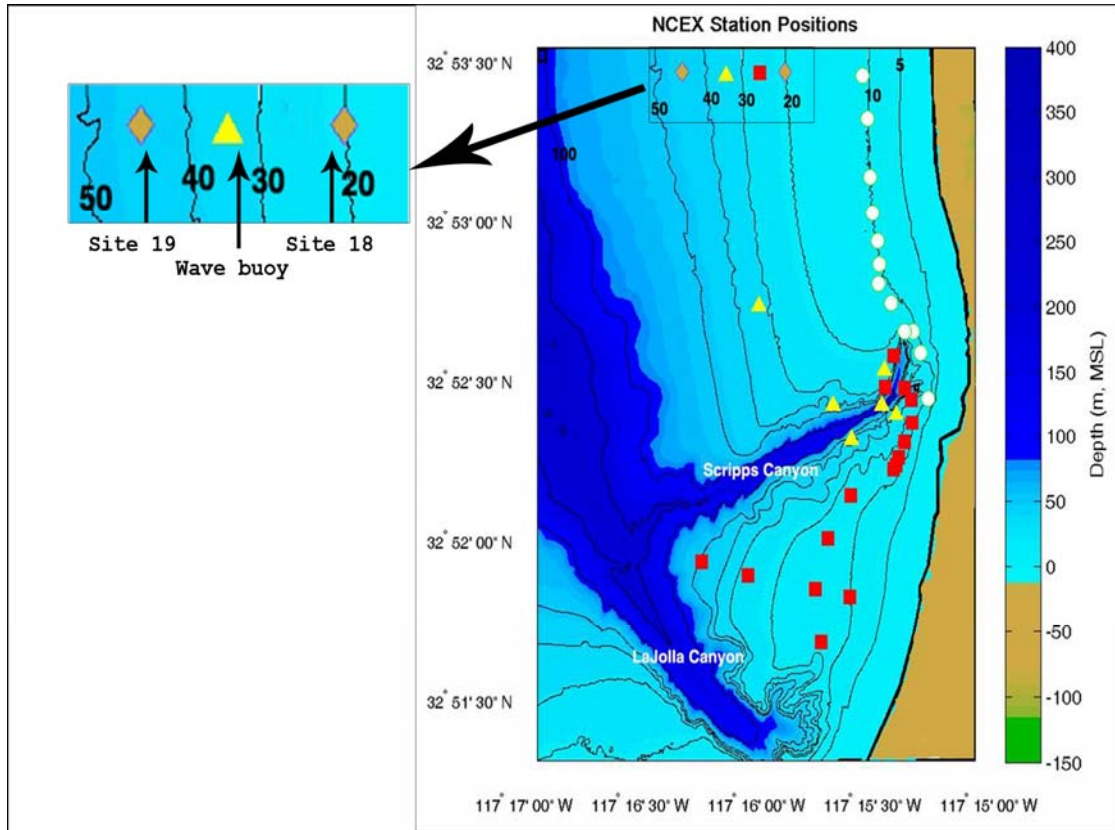


Figure 1. NCEX array plan. Directional Waverider buoys are shown as yellow triangles, bottom pressure recorders are red squares, PUV sensors are white circles, and current profilers are brown diamonds. The inset shows the three instruments used in this study. <http://www.oc.nps.navy.mil/wavelab/ncex.html>, Retrieved October 2006.

## 2. Mooring Configuration

The ADCPs at both sites 18 and 19 were mounted on a Sea-Spider tripod (Figure 2). The Sea-Spider is a fiberglass tripod made by The Oceanscience Group that can

be used for mounting various instrument packages. It weighs close to 200 lbs when lead ballast is attached to each of the tripod feet. Mounted to the Sea-Spider is an acoustic release that releases a pop-up float to enable recovery of the tripod. Data recovery revealed that the tripod at site 19 had fallen over during the first leg (Deployment A, Table 1) resulting in ADCP beams looking horizontally through the water column and rendering the data from this leg not usable. During the second leg (Deployment B) both ADCP's were deployed in a satisfactory configuration for a six week period.

	Site 18	Site 19
Location	32 53.4540 N 117 15.8754 W	32 53.4528 N 117 16.3433 W
Depth	20 m	45 m
Deployment A	09/22/2003 1139 PST- 10/25/2003 1213 PST	No Data
Deployment B	10/27/2003 0801 PST- 12/12/2003 1730 PST	10/27/2003 0900 PST- 12/12/2003 1730 PST
Number of Cells	20	50
Cell Size	1 meter	1 meter
Sampling Rate	2Hz	2Hz
Sample points	8192	8192
Burst Interval	3 hours	3 hours
Bins used	Deployment A: 2,6,9,13,15,17  Deployment B: 2,5,8,11,13,14	2,10,18,26,34,42

Table 1. Configuration and data collection details of ADCPs at sites 18 and 19.

### 3. Velocity Cells

The ADCP divides the water column into depth cells (Figure 3) or bins. There were 20 cells at 1m intervals at site 18, and 45 cells also at 1m intervals at site 19. The acoustic transducers and pressure sensor of the ADCP were approximately 0.6m ( $d_p$ , in Figure 3) above the bottom due to the height of the Sea-Spider. The first cell is actually centered at 1.5 m above the ADCP, or about 2.1 meter above the sea floor. At both sites bins were selected to take measurements throughout the water column (Figure 3 and Table 1). This vertical array of velocity measurements is comparable to mounting individual current meters at these depths. However, unlike individual current meters, the ADCP measures the average velocity over the depth range of each bin as opposed to a single point in space (RDI Manual Primer). Furthermore, different velocity components measured by the four beams are separated in the horizontal, complicating the interpretation of short wavelength components of the surface wave field.



Figure 2. Teledyne Workhorse Sentinel ADCP (upper photo) mounted on Sea-Spider prior to deployment (lower photo). Mounted below the instrument is an extra battery pack. Attached to the front side of the Sea-Spider is the acoustic release assembly with a recovery buoy. (Upper photo from <http://www.rdinstruments.com/sen.html>), Retrieved October 2006.

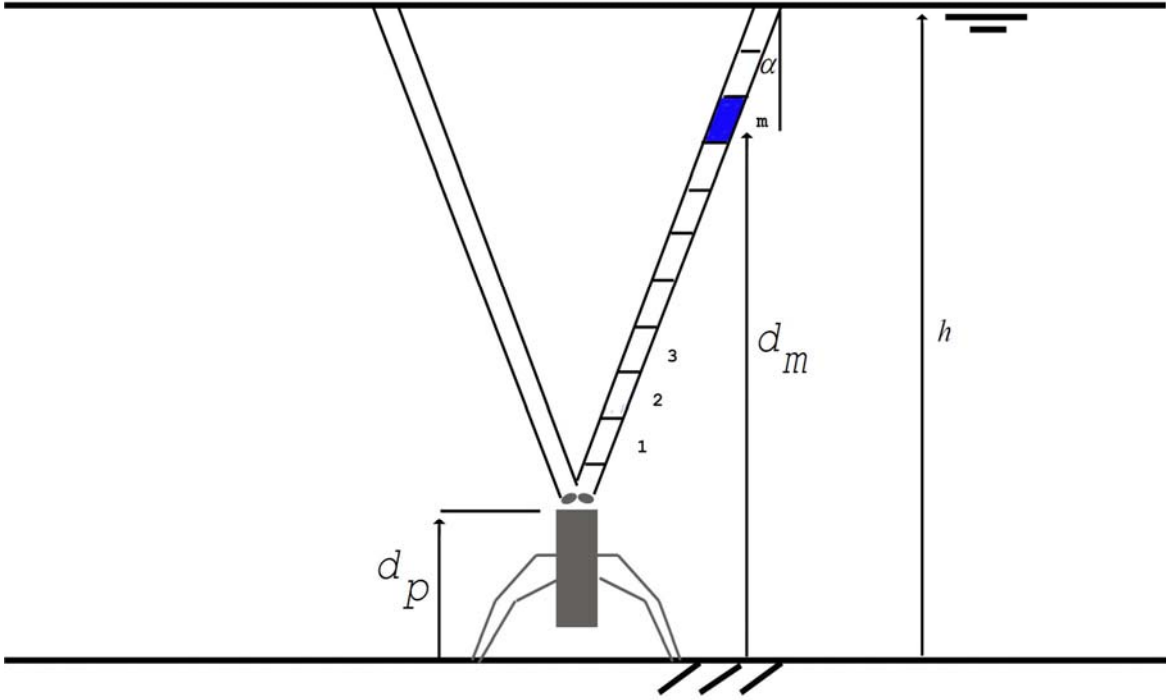


Figure 3. ADCP schematic detailing beams and velocity cells.  $d_p$  is the height of the transducer and pressure sensor above the bed (0.6m).  $d_m$  is the height of cell  $m$  highlighted in blue,  $h$  is the total depth of water,  $m$  is the velocity cell index, and  $\alpha$  is the angle of the beams relative to vertical (20 degrees).

### **III. DATA ANALYSIS**

The ADCP's deployed at sites 18 and 19 provided large data sets. This chapter details the techniques used for quality control, including screening the data for dropouts and correcting these problems where possible.

#### **A. QUALITY CONTROL OF DATA**

Bad velocity data usually associated with dropouts in the Doppler returns are easily identified in the data stream as values of -32768 mm/s. These bad data values were replaced by interpolated points using the cubic spline method. This method is effective for correcting isolated dropouts, but when applied to continuous blocks of bad data or a large fraction of data samples, the artificial smoothing may alter the characteristics of the time series. To avoid biasing the data, a burst was discarded if it included more than two percent bad data or if there was more than five seconds (10 points) of continuous bad data in the burst.

##### **1. Site 18 Data Quality Control**

At site 18, only deployment B was used. Deployment A's 264 bursts were discarded due to consistently bad data in bin 14. The cause of this is not known. The remaining 370 bursts in deployment B were used. In deployment B there were 65 bursts that contained no dropouts (bad values). There were 304 bursts that had some dropouts (that did not exceed the above mentioned criteria) and could be fixed through interpolation. The remaining one burst exceeded the screening criteria and thus was discarded. The remaining 369 "clean" bursts are used for further analysis.

Figure 4 shows example time series from site 18. Panel (a) shows a clean record without a single dropout. Panel (b) shows a typical data record with some dropouts that could be corrected thorough interpolation. The same burst is shown in panel (c) after correcting the dropouts. Finally, panel (d) shows a wave burst with bad data that did not meet the screening criteria and thus was discarded.

## **2. Site 19 Data Quality Control**

There were only 369 bursts available due to lost data in the first half of the ADCP deployment. Applying the same quality control procedures that were applied to site 18 revealed that only one burst did not have a single dropout point, whereas 305 bursts had dropouts that could be corrected through interpolation. The remaining 63 bursts exceeded the screening criteria and could not be used. This resulted in 306 bursts of good data.

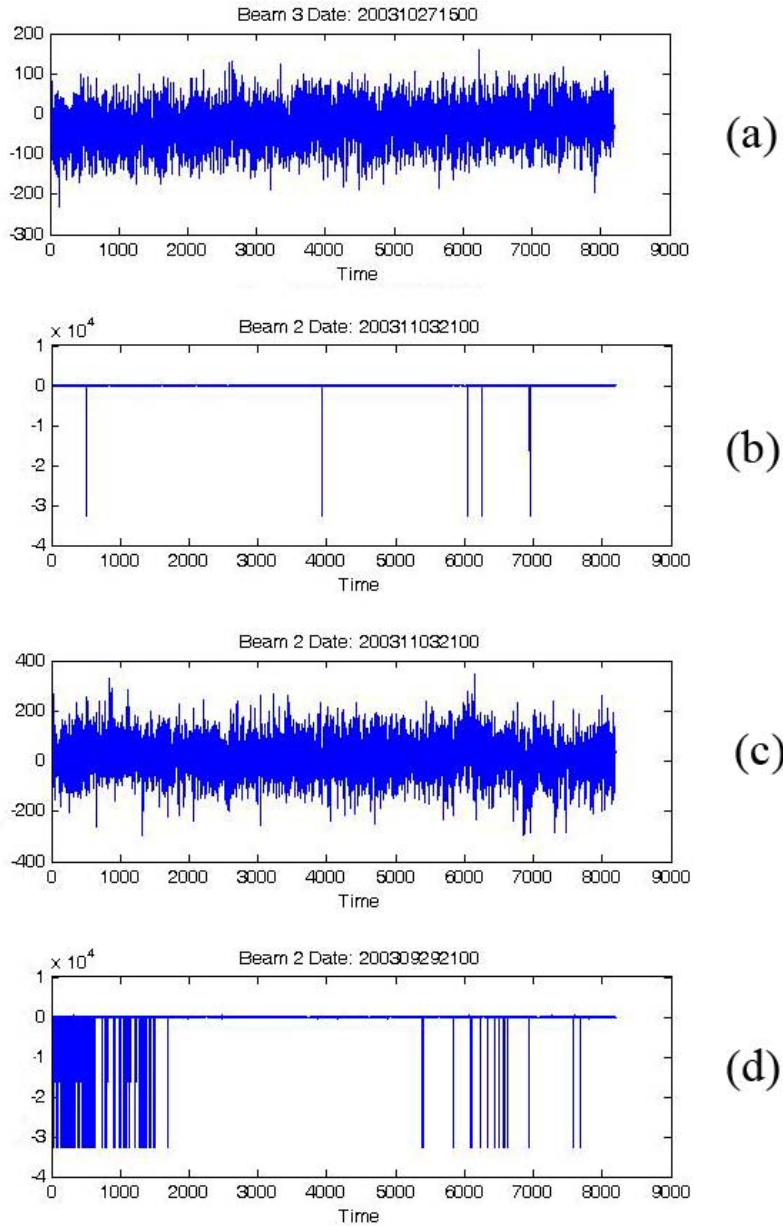


Figure 4. Example wave burst time series (units mm/s) from site 18. From top to bottom: (a) Clean data. (b) A typical burst with some dropouts. (c) The same burst after dropouts were corrected. (d) A burst of low quality data that could not be corrected.

## B. BEAM COMPARISONS

There is redundant information in opposing beams due to the fact they measure the same horizontal velocity component in opposite directions and the same upward

vertical velocity component. If the wave field is assumed to be statistically uniform over the footprint of the ADCP and (from linear wave theory) the horizontal and vertical components are in quadrature, then it follows that the velocity variances measured by opposing beams are equal. Thereby, comparing the velocity variances of opposing beams provides a consistency check of the ADCP performance.

Figure 5 compares velocity variances at site 18 from opposing beams 1 and 2 (panel (a)) and beams 3 and 4 (panel (b)). The top panel shows the highest bin (i.e., furthest from the sensor) (bin 14) and the bottom panel the lowest bin (bin 2). This comparison clearly shows that as the measurements are taken further away from the sea floor the agreement becomes excellent. Bin 2 shows degraded agreement between the beams that is probably due to its proximity to the sea bed resulting in bottom interference.

Beam comparisons at site 19 shown in Figure 6 follow the same pattern as seen in Figure 5. Evident here are the effects of attenuation in deep water. The upper bins for all beams show energetic velocity signals observed near the surface and good agreement between opposing beam velocities. On the other hand, at the lower bins, the wave velocity field is strongly attenuated and the measured variances are close to the instrument noise floor.

### **C. NOISE FLOOR**

Since most of the wave energy is concentrated at the lower frequencies, and high frequency waves with relatively short wavelengths are attenuated over the water column, the spectral levels observed at higher frequencies usually

roll-off to the noise floor. Therefore, examining the high-frequency spectral levels is useful to establish the instrument noise level, providing a final quality check.

Frequency spectra were computed from the velocity time series using a standard Fast Fourier Transform technique. A Hamming window was applied to segments with a length of 256 points (128s) and 50 % overlap to boost the confidence intervals of the spectral estimates. The velocity spectra were then integrated from 0.5 Hz to the Nyquist frequency at 1 Hz. In this range the wave signal levels are usually well below the instrument noise levels, and thus the integrated velocity variances provide an estimate of the noise floor. The high frequency velocity variances observed at site 18 are shown in Figure 7, both before (a) and after (b) the data were corrected for drop outs. The corrected data has consistently low variances of about 800 (mm/s)<sup>2</sup>, which corresponds to a noise level (assuming the same level over the entire 0-1 frequency range) of about 4 cm/s.

At site 19 (Figure 8) the lower bins show similar low noise levels. However, noise levels are higher in the upper bins, in particular the top velocity cell often shows variances as high as a 10000(mm/s)<sup>2</sup>, or a noise level around 15 cm/s.

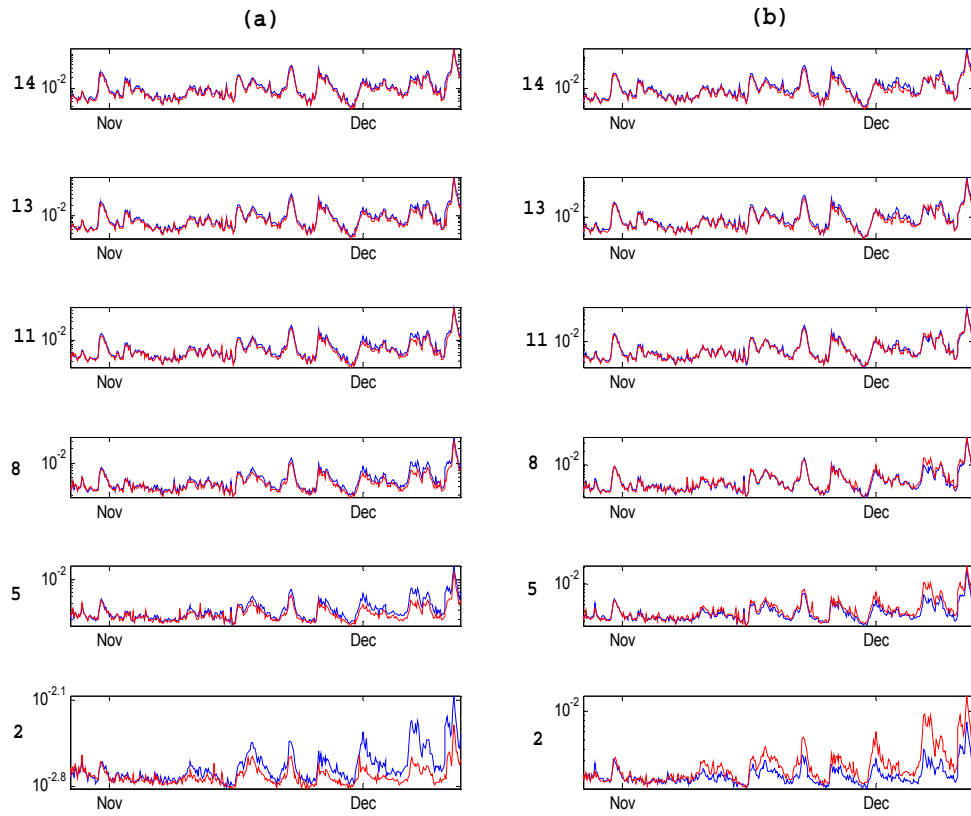


Figure 5. Site 18 velocity variances (units  $(\text{m/s})^2$ ), from opposing beams (a) 1, 2 and (b) 3, 4. Results from all six bins are shown, from near the surface (top) to the near sea floor (bottom).

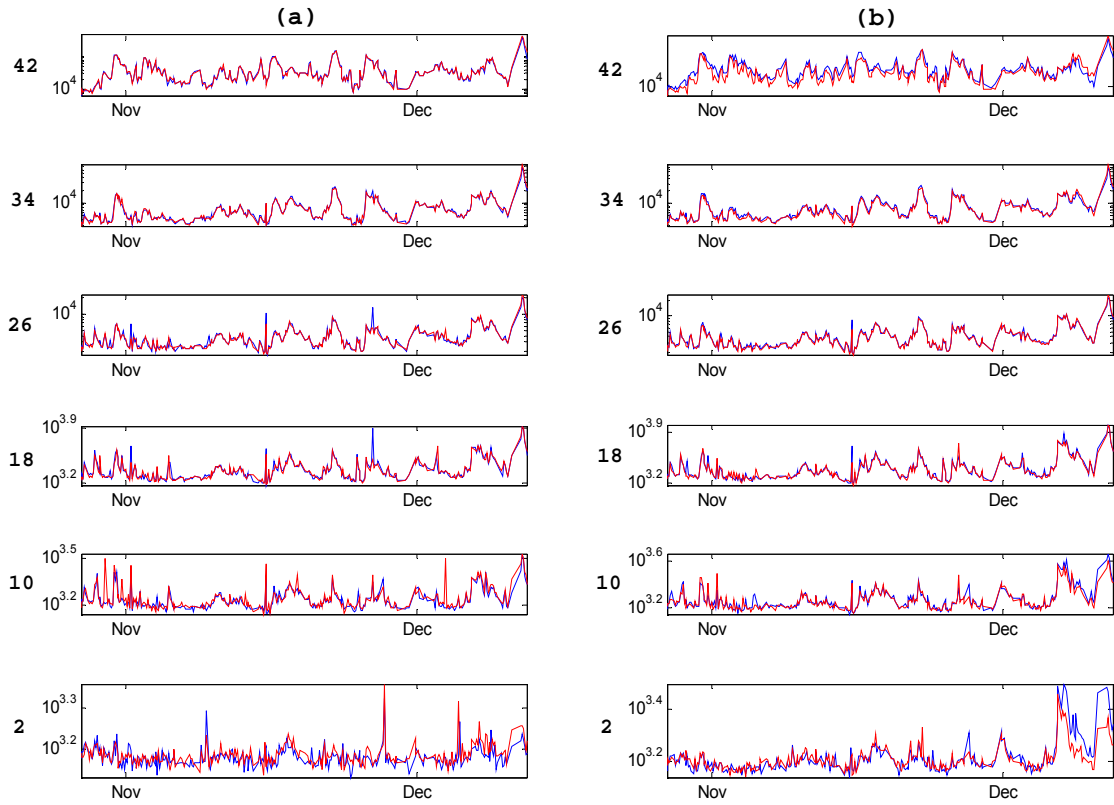


Figure 6. Site 19 velocity variances (units  $(\text{m/s})^2$ ). (Same format as Figure 5).

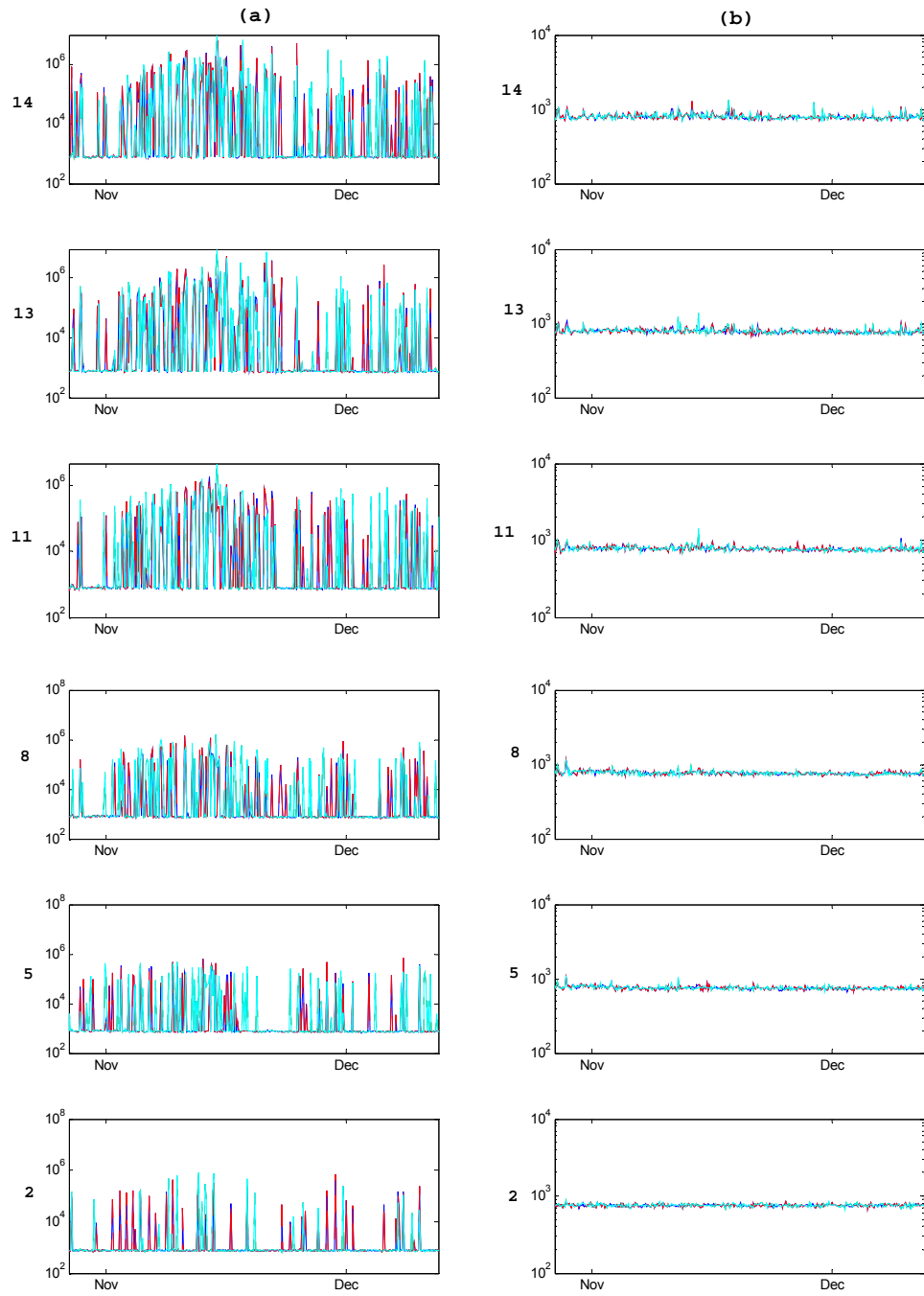


Figure 7. Site 18 high frequency velocity variances (units  $(\text{mm/s})^2$ ) of all four beams. Uncorrected data is shown in (a) and corrected data in (b). The top panels show the uppermost bin, the bottom panels the lowest bin.

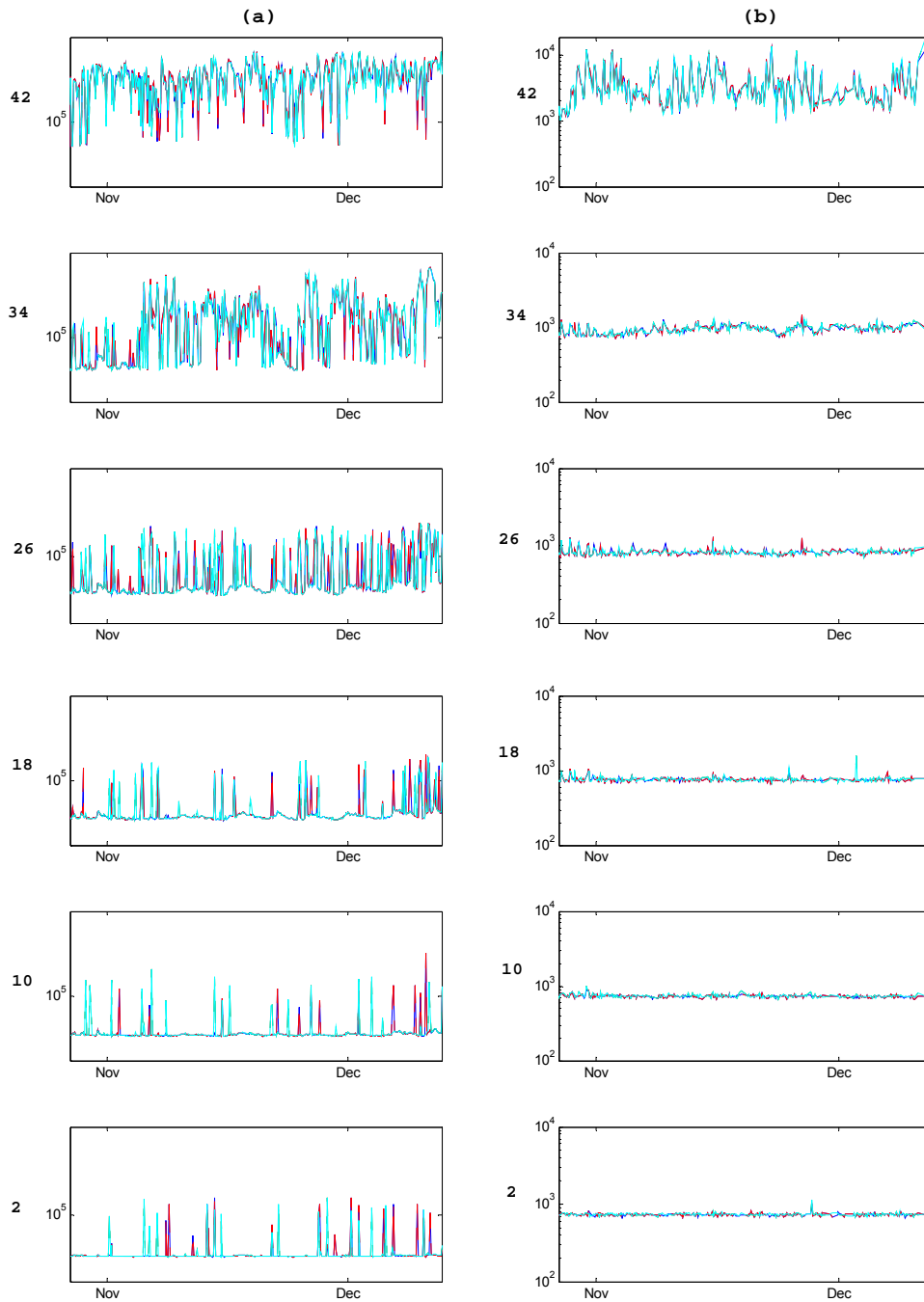


Figure 8. Site 19 high frequency velocity variances (units  $(\text{mm/s})^2$ ). (Same format as Figure 7).

THIS PAGE INTENTIONALLY LEFT BLANK

#### IV. VERIFICATION LINEAR TRANSFER FUNCTION

The ADCP collects both pressure and velocity measurements that are related through a frequency-dependent linear wave theory transfer function. Therefore, the accuracy of the ADCP velocity measurements can be verified by comparing the ADCP derived pressure spectrum based on the theoretical transfer function with the directly measured pressure spectrum.

##### A. PRESSURE-VELOCITY TRANSFER FUNCTION

According to linear theory, the sum of the ADCP velocity spectra measured by the four beams at an arbitrary depth cell  $m$  (Figure 2)  $E_1^m + E_2^m + E_3^m + E_4^m$  is related to the measured pressure spectrum  $E_{p(f)}$ .

$$E_p(f) = \left[ \left( \frac{2\pi f}{gk} \right)^2 \frac{\cosh^2 kd_p}{2 \sin^2 \alpha \cosh^2 kd_m + 4 \cos^2 \alpha \sinh^2 kd_m} \sum_{n=1}^4 E_n^m(f) \right]$$

Here  $g$  is acceleration of gravity,  $k$  is the wavenumber given by the linear dispersion relation,  $\alpha$  is the angle of the beam relative to the vertical,  $d_m$  is the height of the velocity cells above the sea floor and  $d_p$  is the height of the pressure sensor above the seafloor (see Figure 2).

##### B. SPECTRAL COMPARISONS

Example comparisons of velocity-derived and directly measured pressure spectra are shown in figures 9-12. In each case pressure spectra inferred from velocity measurements at all six depth cells are compared with the measured pressure spectrum. Figure 9 shows an example of high quality data collected at the shallower (site 18) ADCP. The spectrum features a dominant swell peak at 0.07

Hz and a lower frequency 'surf beat' peak at 0.02 Hz. At all velocity cells there is excellent agreement with the pressure observations across both spectral peaks. Only at frequencies higher than about 0.15 Hz do the spectra diverge.

There are many cases of velocity data that passed the quality control criteria but nonetheless showed poor agreement with the pressure data. Two examples at site 18 are shown in figures 10 and 11. In Figure 10 the velocity derived pressure spectra of all 6 cells greatly exceed the measured spectral levels across the entire 0-0.25 Hz frequency range. The causes of these large errors are large spikes in the velocity time series observed across all 4 beams (lower panel Figure 10).

Figure 11 shows an example of another type of error in the data that caused poor agreement between estimated pressure and directly measured pressure. In this case, the time series of beams 1 and 4 show a large shift in the mean velocity (at different times) that in the spectral analysis produces spurious low frequency levels.

Figure 12 shows a comparison of the velocity-inferred and directly measured pressure spectra at the deeper site 19. In the frequency range 0.05 to 0.12 Hz that contains the dominant swell energy, the agreement is good at all depth cells with the exception of cell 2 (closest to the ADCP) where the velocity derived spectra are too high at frequencies above 0.09 Hz. This discrepancy may be caused by attenuation of waves through the water column and the associated degraded signal to noise ratio near the bottom.

### C. VARIANCE COMPARISONS

Comparisons of directly measured and velocity-derived pressure variances for the entire deployment are shown in the top panel of figures 13 (site 18) and 14 (site 19). At site 18 the agreement is generally good with the exception of a few days around the 15<sup>th</sup> of November when there were less energetic wave conditions. These discrepancies are likely the result of low signal to noise ratios. Site 19 also shows poor agreement (Figure 14) around the 15<sup>th</sup> of November, consistent with low signal to noise ratios. Overall the errors at site 19 are larger than at site 18, and especially the lowest bin shows poor agreement with the pressure measurements, indicating that the hydrodynamic attenuation at this deeper site is a problem for ADCP wave measurements in the lower part of the water column.

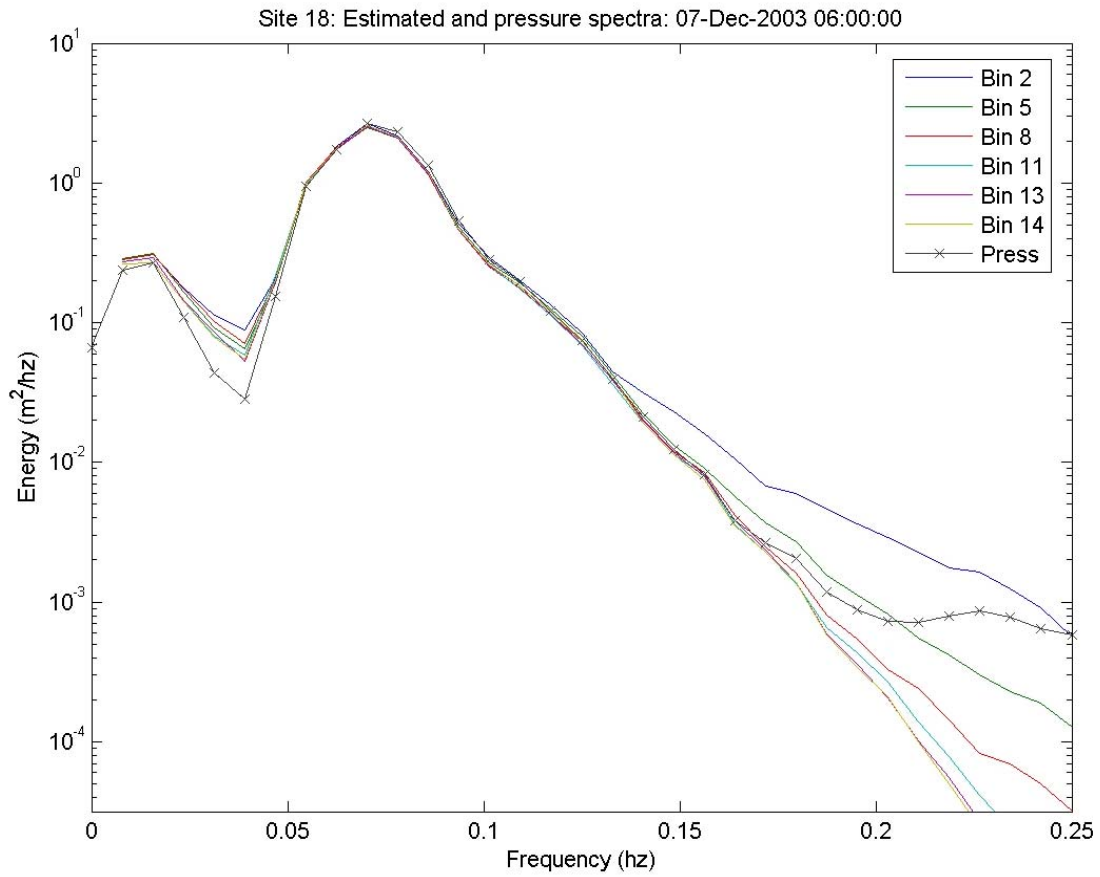


Figure 9. Comparison of bottom pressure spectrum at site 18 estimated from ADCP velocity measurements at 6 depth cells and the directly measured pressure spectrum.

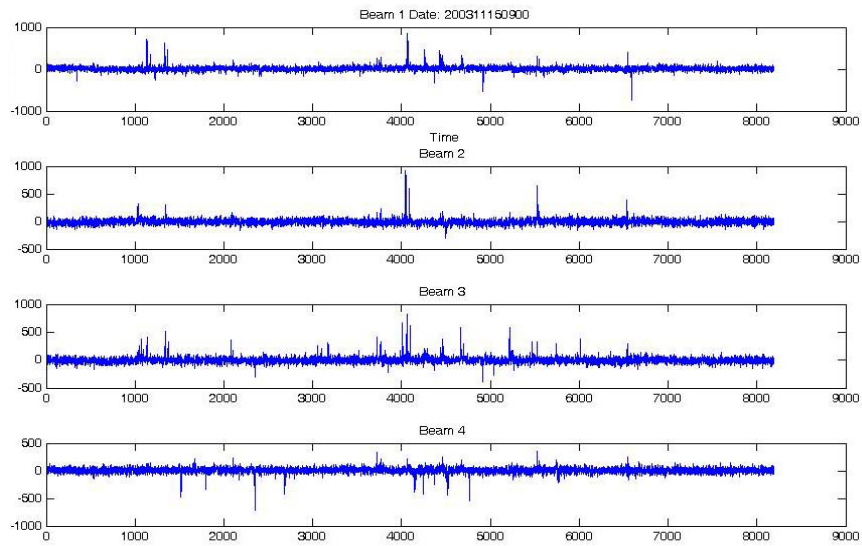
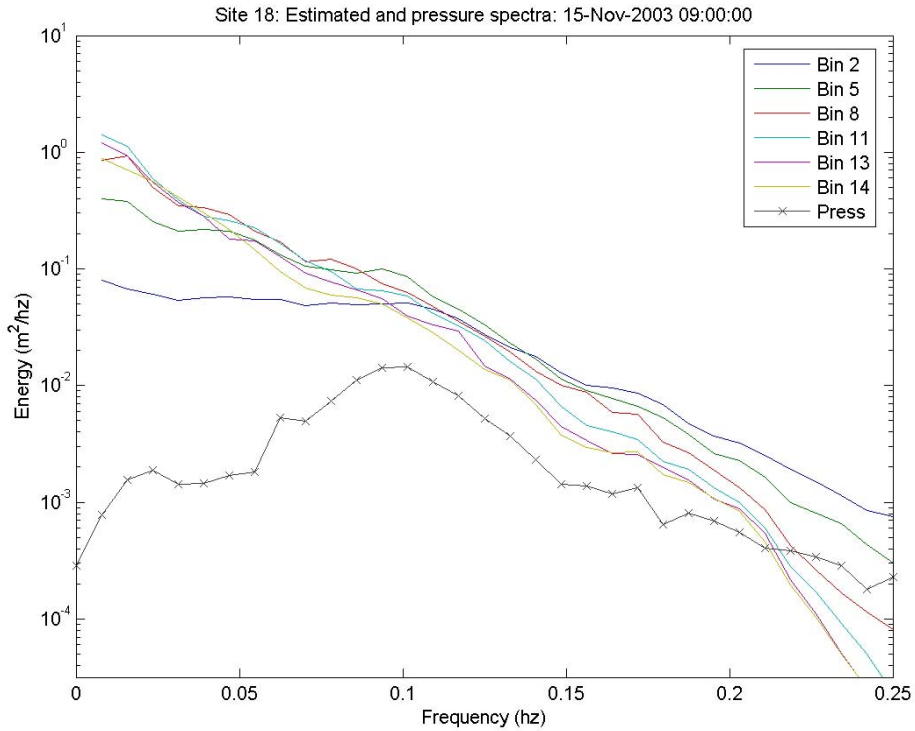


Figure 10. Comparison of bottom pressure spectrum at site 18 predicted from ADCP velocity measurements with directly measured pressure. The lower panel shows time series from one of the cells (5) with many spikes that degrade the spectrum estimate.

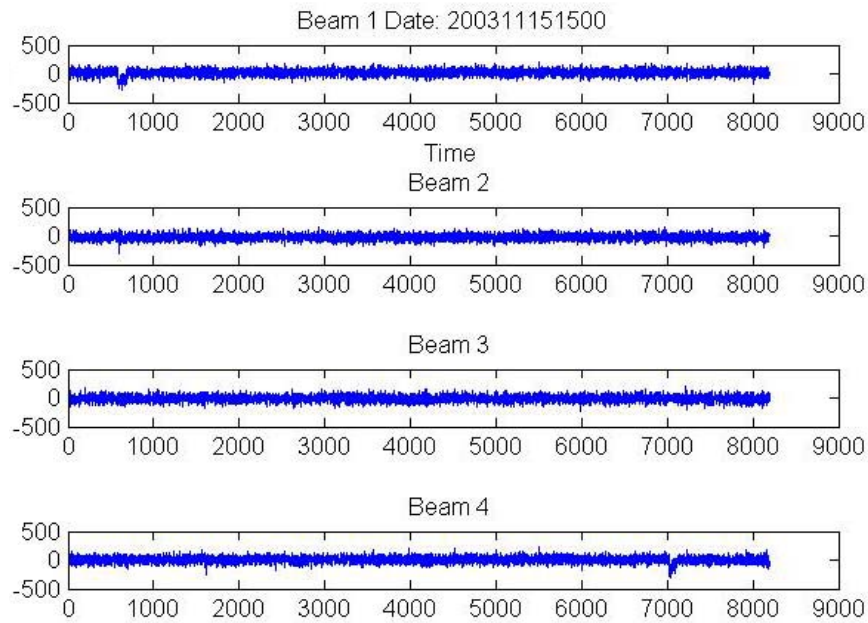
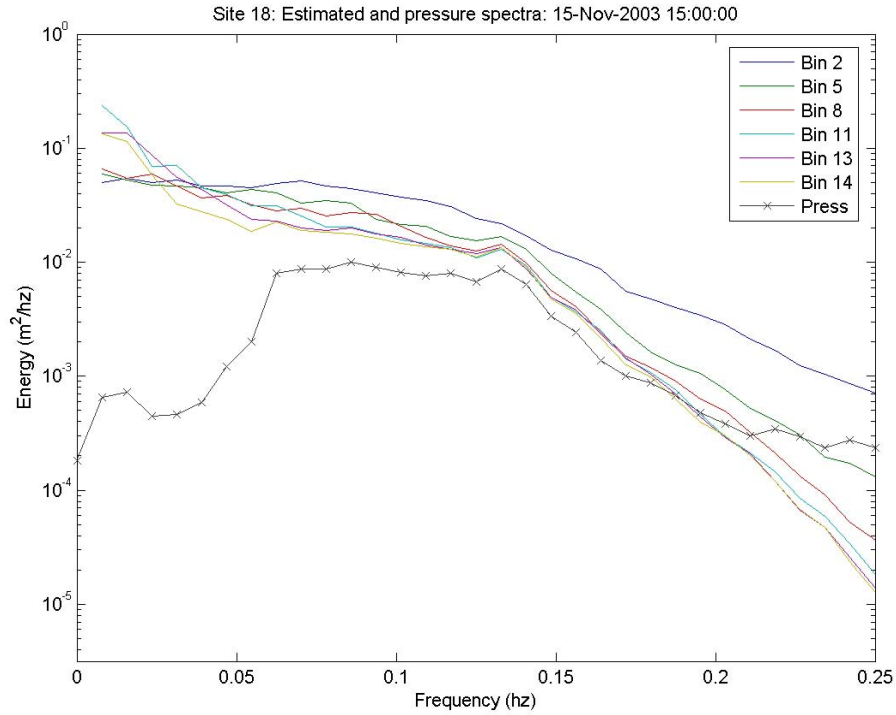


Figure 11. Comparison of bottom pressure spectrum at site 18 predicted from ADCP velocity measurements with the directly measured pressure spectrum. Bottom panel: Time series of cell 11 that show large shifts in beams 1 and 4.

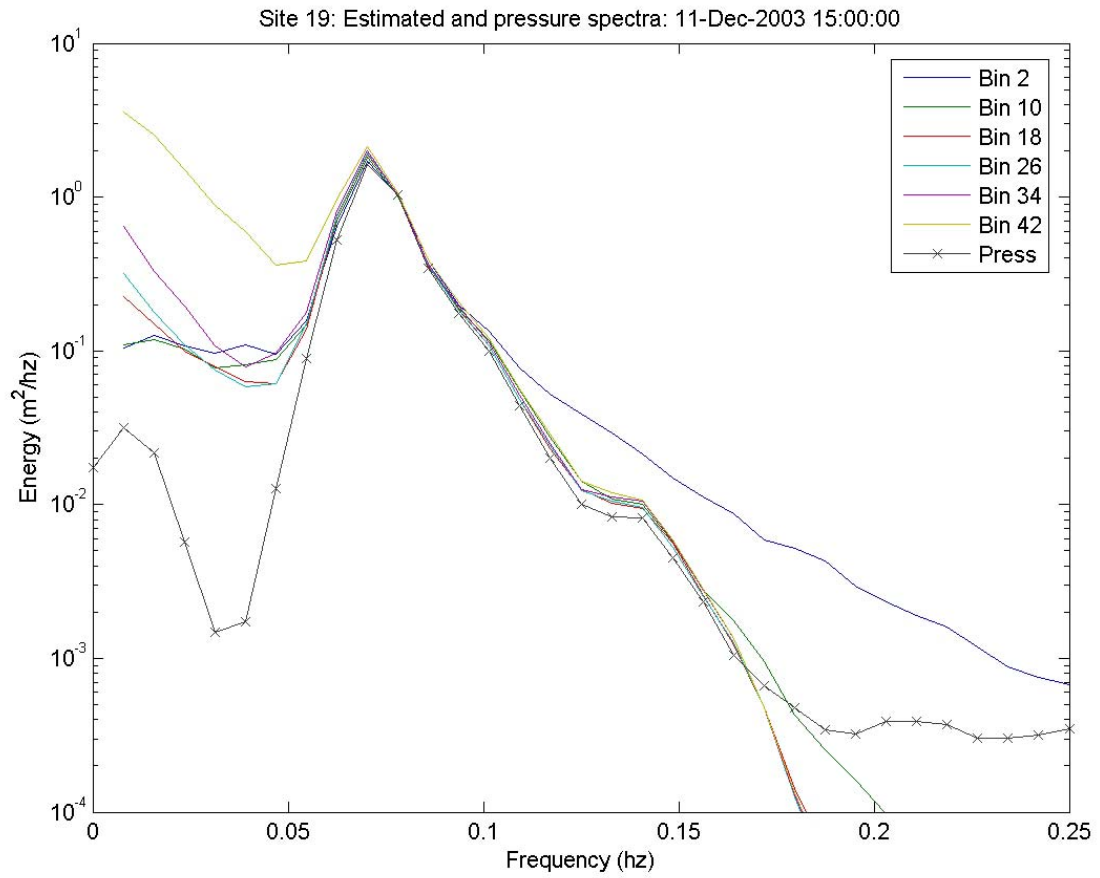


Figure 12. Comparison of bottom pressure spectrum at site 19 predicted from ADCP velocity measurements and directly measured pressure. (Same format as Figure 9).

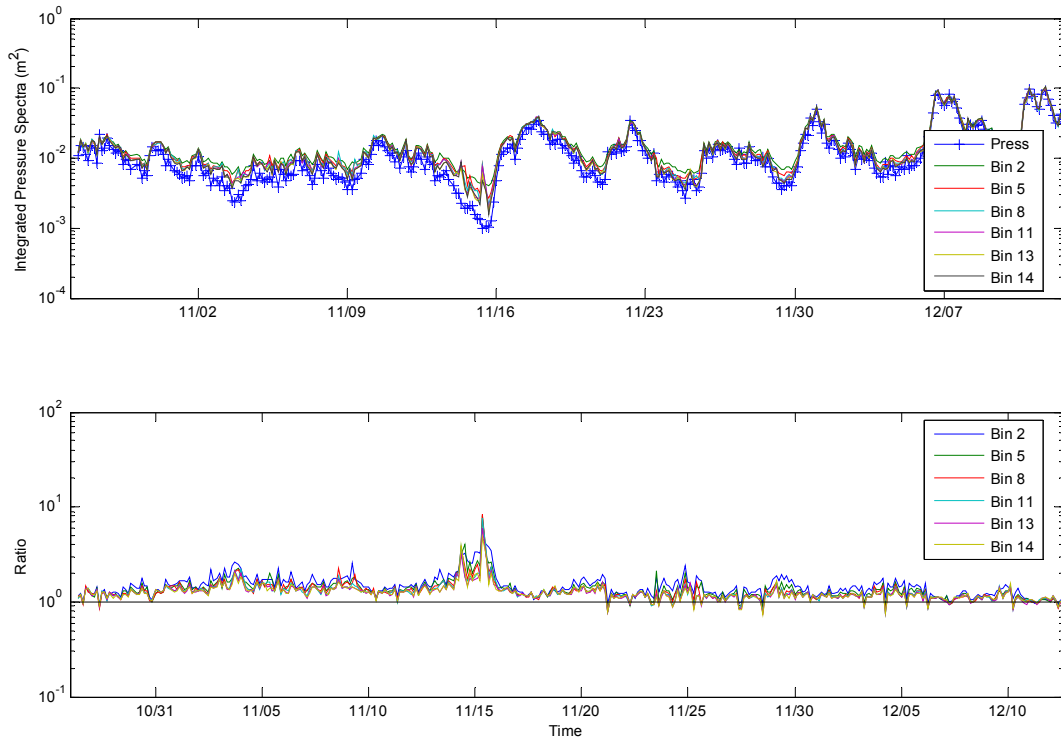


Figure 13. Comparison of ADCP-derived bottom pressure variances at site 18 with directly measured pressure variance. The top panel shows estimates for all six depth cells. The bottom panel shows the ratio between predicted and measured pressure variance.

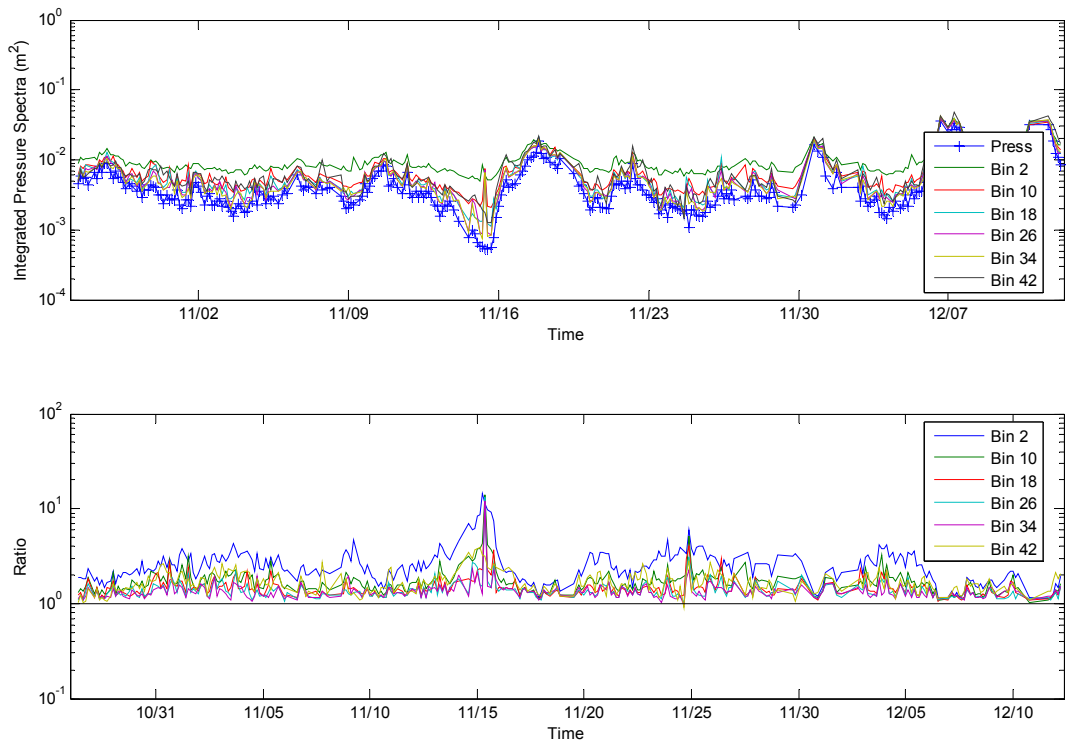


Figure 14. Comparison of ADCP-derived bottom pressure variances at site 19 with directly measured pressure variance. (Same format as Figure 13).

THIS PAGE INTENTIONALLY LEFT BLANK

## V. DIRECTIONAL WAVE SPECTRA

This chapter details the verification of directional wave information extracted from ADCP velocity measurements using independent estimates obtained with a nearby Datawell Waverider buoy. First the method to estimate surface height spectra and directional distributions of wave energy is reviewed. Next, three case studies are presented that illustrate the capabilities and limitations of the ADCP.

### A. ESTIMATION TECHNIQUE

Estimates of wave frequency-directional spectra can be obtained from multi-component observations using a variety of techniques (e.g. Davis and Regier, 1977; Pawka, 1983; Herbers and Guza, 1990). The following analysis method, specifically designed for ADCP measurements was provided by Professor Thomas H.C. Herbers (manuscript in preparation).

#### 1. The Frequency-Directional Wave Spectrum

The surface elevation function  $\eta$  of a random, homogeneous wave field can be expressed as a superposition of plane waves with different frequencies  $\omega$  and propagation directions  $\theta$ :

$$\eta(\vec{x}, t) = \sum_{\omega} \sum_{\theta} A_{\omega, \theta} \exp \left[ i \left( \vec{k} \cdot \vec{x} - \omega t \right) \right]. \quad (1)$$

The wavenumber vector in (1) is defined as  $\vec{k} = (k \cos \theta, k \sin \theta)$  with  $k$  obeying the linear gravity wave dispersion relation  $\omega^2 = gk \tanh(kh)$  where  $\omega = 2\pi f$  is the angular frequency,  $g$  is gravity,  $h$  the water depth, and  $k$  has the same sign as  $\omega$ . The complex amplitudes obey the symmetry relation  $A_{-\omega, \theta} = (A_{\omega, \theta})^*$  where  $*$  denotes the complex conjugate.

The sea surface amplitudes  $A_{\omega,\theta}$  are assumed to be statistically independent. In the limit of small separation of the frequencies( $\Delta\omega$ )and directions( $\Delta\theta$ ), their statistics can be described by a continuous spectrum

$$\langle |A_{\omega,\theta}|^2 \rangle \equiv E(\omega,\theta)\Delta\omega\Delta\theta \quad (2)$$

where  $\langle \rangle$ denotes the expected value. It follows from (1) and (2) that the integral of the frequency-directional spectrum  $E(\omega,\theta)$  over all frequencies and directions equals the surface elevation variance

$$\langle \eta^2 \rangle = \int_{-\infty}^{\infty} d\omega \int_0^{2\pi} d\theta E(\omega,\theta). \quad (3)$$

## 2. Transfer Functions for ADCP Velocity Measurements

The ADCP velocity measurements are related to the sea surface elevation (1) through linear transfer functions:

$$V_n^m(t) = \sum_{\omega} \sum_{\theta} G_n^m(\omega,\theta) A_{\omega,\theta} \exp(-i\omega t) \quad (4)$$

where the subscript  $n$  indicates the beam number (1 through 4) and the superscript  $m$  the velocity cell index. According to linear theory the transfer function  $G_n^m$  is given by

$$G_n^m(\omega,\theta) = \frac{gk \exp(i\vec{k} \cdot \vec{x}_n^m)}{\omega \cosh(kh)} \{ \sin \alpha \cosh(kd_m) \cos(\theta - \theta_n) - i \cos \alpha \sinh(kd_m) \} \quad (5)$$

where  $\vec{x}_n^m$  is the horizontal position vector of the velocity cell,  $d_m$  is the height of cell  $m$  above the seafloor,  $\theta_n$  is the orientation of beam  $n$  in the horizontal plane relative to the  $x$ -axis, and  $\alpha$  is the angle of the beams relative to the vertical.

The covariance of any pair of velocity measurements can be expressed as (using (2) and (4))

$$\langle V_n^m(t) V_r^s(t) \rangle \equiv \int_{-\infty}^{\infty} d\omega C_{V_n^m V_r^s}(\omega) = \int_{-\infty}^{\infty} d\omega \int_0^{2\pi} d\theta G_n^m(\omega, \theta) (G_r^s(\omega, \theta))^* E(\omega, \theta),$$

yielding a relationship between the cross-spectrum  $C_{V_n^m V_r^s}$  and the wave spectrum  $E$

$$C_{V_n^m V_r^s}(\omega) = \int_0^{2\pi} d\theta G_n^m(\omega, \theta) (G_r^s(\omega, \theta))^* E(\omega, \theta). \quad (6)$$

The wave spectrum can be decomposed in a frequency spectrum  $E(\omega)$  and a directional distribution at each frequency  $S(\theta; \omega)$

$$E(\omega, \theta) \equiv E(\omega) S(\theta; \omega) \quad (7)$$

where

$$\int_0^{2\pi} d\theta S(\theta) = 1. \quad (8)$$

The objective of the present analysis is to obtain robust estimates of  $E(\omega)$  and  $S(\theta; \omega)$  from the velocity cross-spectra  $C_{V_n^m V_r^s}(\omega)$ .

### 3. Estimate of the Frequency Spectrum

Owing to the orthogonal beam configuration, the sum of the auto-spectra is independent of direction and yields a direct estimate of the wave frequency spectrum:

$$\hat{E}(\omega) = \frac{\omega^2 \cosh^2(kh) \sum_n \sum_m C_{v_n v_m}(\omega)}{g^2 k^2 \sum_m \{2 \sin^2 \alpha \cosh^2(kd_m) + 4 \cos^2 \alpha \sinh^2(kd_m)\}} \quad (9)$$

Other combinations of the auto spectra can be used to estimate  $E(\omega)$ . The present formulation using equal weights has the advantage that it tends to reject velocity measurements with low signal to noise ratios. This is important for high frequency waves that are attenuated over the water column and may not be reliably detected by the lower velocity cells. For these short wavelength, high frequency waves the estimate (9) is dominated by the larger signals in the upper velocity cells, and thus not seriously degraded by the noisy lower cells. On the other hand for long wavelength waves with relatively weak vertical motions and horizontal flows that are uniform over the water column, all depth cells contribute equally to (9), yielding a robust estimate of  $E$  that uses all measurements. Further improvements to (9) may be possible by removing the estimated bias resulting from instrument noise.

#### 4. Estimate of the Directional Distribution

Normalizing (6) by the frequency spectrum estimate  $\hat{E}$  (using (7)) yields a relation between the ADCP velocity cross-spectra and the directional distribution of wave energy  $S(\theta)$ . This set of equations can be written compactly as

$$\int_0^{2\pi} d\theta \mathbf{g}(\theta) S(\theta) = \mathbf{d} \quad (10)$$

where the elements of vector  $\mathbf{d}$  are the normalized cross-spectra  $C_{V_n^m V_r^s} / \hat{E}$ , and the elements of vector  $\mathbf{g}$  contain the products  $G_n^m (G_r^s)^*$  of the corresponding transfer functions.

The directional distribution of wave energy is often described by a simple cosine-power (Figure 15) function of the form:

$$\hat{S}(\theta) = c_N \cos^{2s} \left( \frac{\theta - \bar{\theta}}{2} \right) \quad (11)$$

where  $\bar{\theta}$  is the mean wave direction, the parameter  $s$  controls the width of the distribution, and  $c_N$  is a normalization constant. The directional spread  $\sigma$ , defined here as the half-width of the directional distribution at half-maximum power, is related to  $s$  by

$$s = \log(1/2) / [2 \log(\cos(\sigma/2))]. \quad (12)$$

The simple parametric form (11) used here is readily extended to more complex (e.g. double-peaked) functions that allow for the representation of a bi-modal wave field (e.g. a wind sea in the presence of swell)

The free parameters of  $\hat{S}$  can be estimated by fitting the distribution to the observed cross-spectra (10). To quantify the goodness of fit, a misfit  $\boldsymbol{\varepsilon}$  is defined as the difference between the observed cross-spectra and the model  $\hat{S}$ :

$$\boldsymbol{\varepsilon} \equiv \mathbf{d} - \int_0^{2\pi} d\theta \mathbf{g}(\theta) \hat{S}(\theta) \quad (13)$$

An optimal model  $\hat{S}$  that best fits the observations is obtained by selecting the parameters that minimize the  $l^2$ -norm  $|\boldsymbol{\varepsilon}| = \sqrt{\boldsymbol{\varepsilon} \cdot \boldsymbol{\varepsilon}}$ . There are only two free parameters  $\bar{\theta}$  and  $s$ . The normalization constant follows from the unit integral constraint (8). A global minimum of  $|\boldsymbol{\varepsilon}|$  can be readily determined by evaluating  $\boldsymbol{\varepsilon}$  for all possible combinations of  $\bar{\theta}$  and  $s$ .

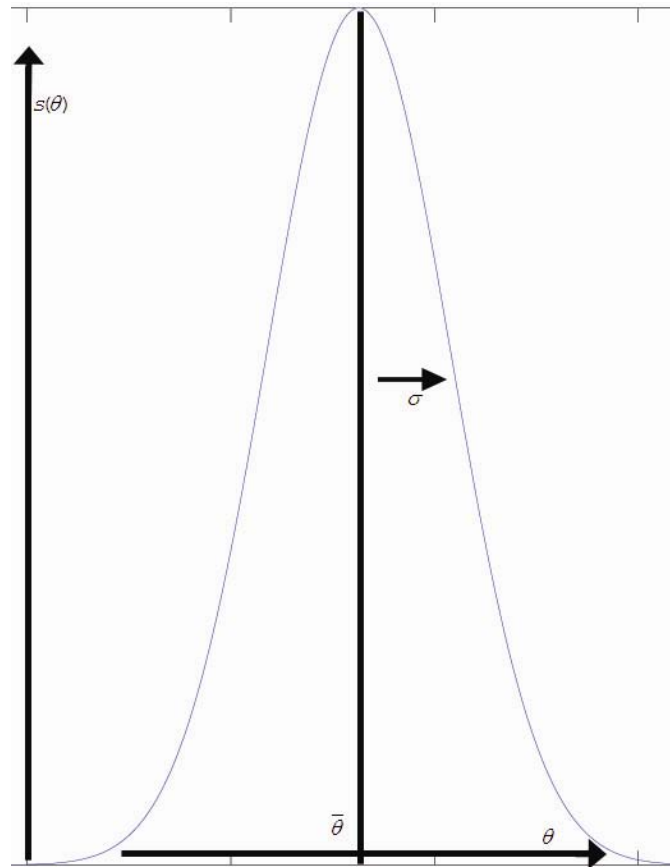


Figure 15. Power cosine model showing the directional distribution of wave energy where  $\sigma$  is the directional spread (i.e., half-width of the distribution) and the mean wave direction is denoted by  $\bar{\theta}$ .

## B. CASE STUDIES

Three case studies were selected for further analysis. An attempt was made to select cases that include a range of swell directions but this was not possible because western swells dominated the entire data set due to offshore refraction effects (Figures 16 and 17). December's ADCP data were not used because the wave buoy was out of operation after December 1<sup>st</sup>.

In each case the wave frequency spectrum  $E(f)$ , mean direction  $\bar{\theta}(f)$ , and directional spread  $\sigma(f)$  were estimated using the technique described previously in the chapter. The ADCP estimates are compared to observations of a Directional Waverider buoy located mid-way between the two ADCP sites (Figure 1).

### 1. October 30<sup>th</sup> 1800 PST

The first case study, taken at the end of October, is dominated by a 15 second swell with a significant wave height of about 0.6m (Figure 16). The upper panel in Figure 18 shows the surface height spectrum comparison between the ADCP's and the wave buoy. Overall the agreement between the ADCP and wave buoy is poor, especially at the lower and higher frequencies away from the dominant swell peak. The agreement is much worse for the deeper site 19 than for the shallower site 18, probably owing to the low signal to noise ratio in these benign conditions.

The mean direction estimate  $\bar{\theta}$  at site 18 is compared to the buoy estimate in the middle panel. The magenta dotted lines ( $\bar{\theta}+\sigma$  upper line,  $\bar{\theta}-\sigma$  lower line) illustrate the width of the directional distribution. The observed

mean directions vary between about  $250^\circ$  at the swell peak to about  $280^\circ$  at higher frequencies and are in excellent agreement with the wave buoy estimates. The directional spreading values range from  $\sigma=10-30^\circ$  and are fairly uniform over the entire frequency range.

The bottom panel shows the mean direction comparison at site 19. Again, there is excellent agreement with the wave buoy estimate, but more directional spreading is observed than at site 18, probably due to the location in deeper water where waves are less affected by refraction and or errors owing to higher noise levels. Overall, this case illustrates that the dominant wave direction can be reliably extracted from the ADCP measurements despite the high noise levels.

## **2. November 17<sup>th</sup> 0000 PST**

The second case study (Figure 19) features two swell peaks with frequencies of about 0.06 Hz and 0.09 Hz (top panel). It is also a more energetic case than case I, with a significant wave height of about 1 m. The wave buoy and ADCP surface height spectra are in good agreement, especially for the shallower instrument at site 18. However, the spectrum estimate from site 19 is biased high at the higher frequencies ( $> 0.013$  Hz).

Again the mean direction comparisons show excellent agreement. Notice that at both sites 18 and 19, as is often observed in ocean wave spectra, the directional distribution is narrowest at the energetic swell peaks.

## **3. November 22<sup>nd</sup> 1800 PST**

The third and final case study is the most energetic case, a local wind sea, with a significant wave height of about 1.7 m and a 7 second peak period. The surface height

spectra in Figure 20 generally show good agreement between the ADCPs and the wave buoy. Again, the agreement is better at the lower frequencies between .06 and 0.1 Hz. As with the other two case studies the ADCP's ability to measure mean wave directions appears to be robust. Narrow directional spreading is again evident across a wide frequency range, demonstrating the high degree of coherence in the ADCP measurements.

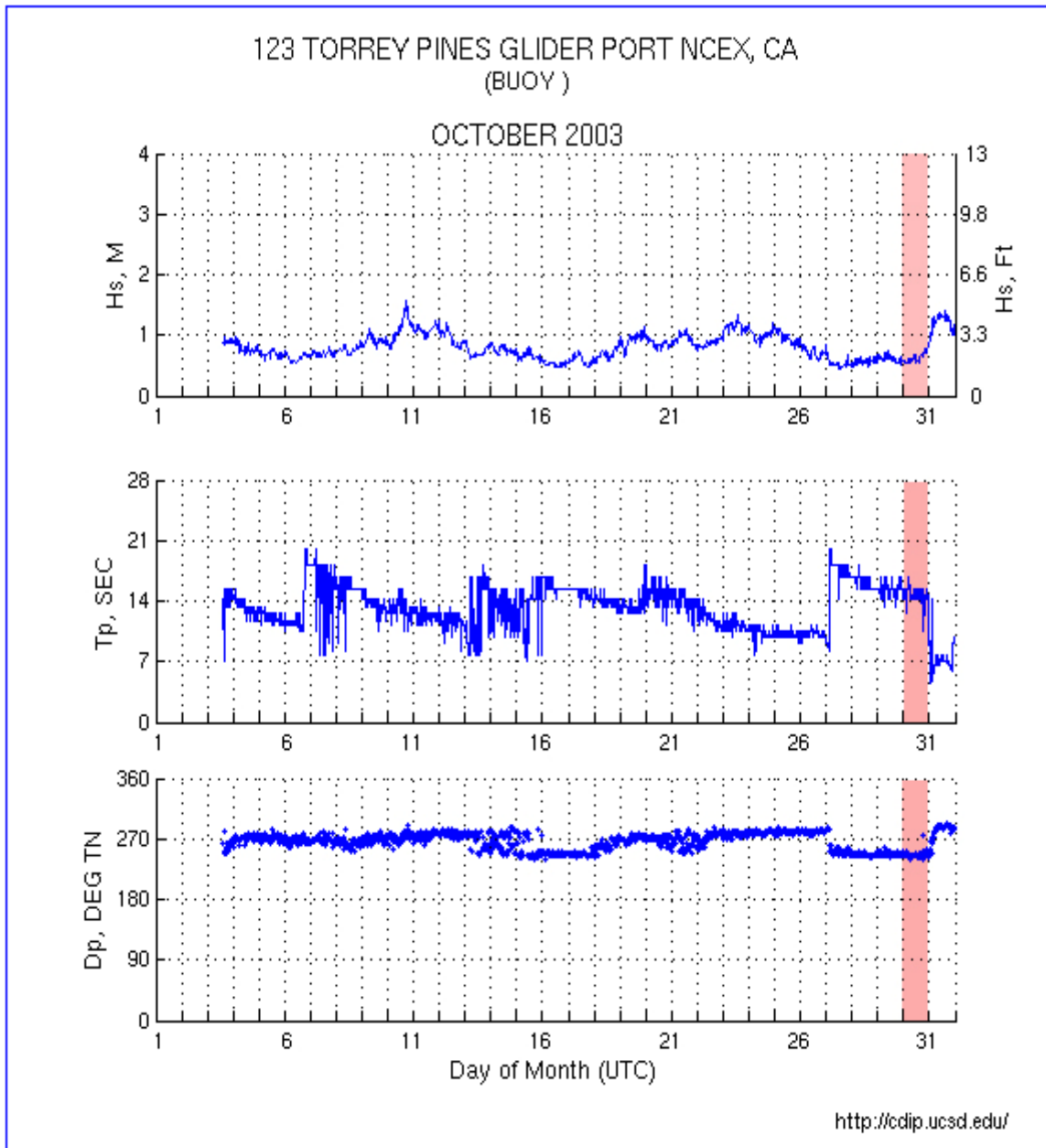


Figure 16. October 2003 wave statistics compendium plot taken from the Coastal Data Information Program (CDIP) website. The location of the buoy (deployed as part of the NCEX experiment) is shown in Figure 1. From top to bottom: significant wave height, peak period, and dominant wave direction. Highlighted in red is the first case study October 30<sup>th</sup>.

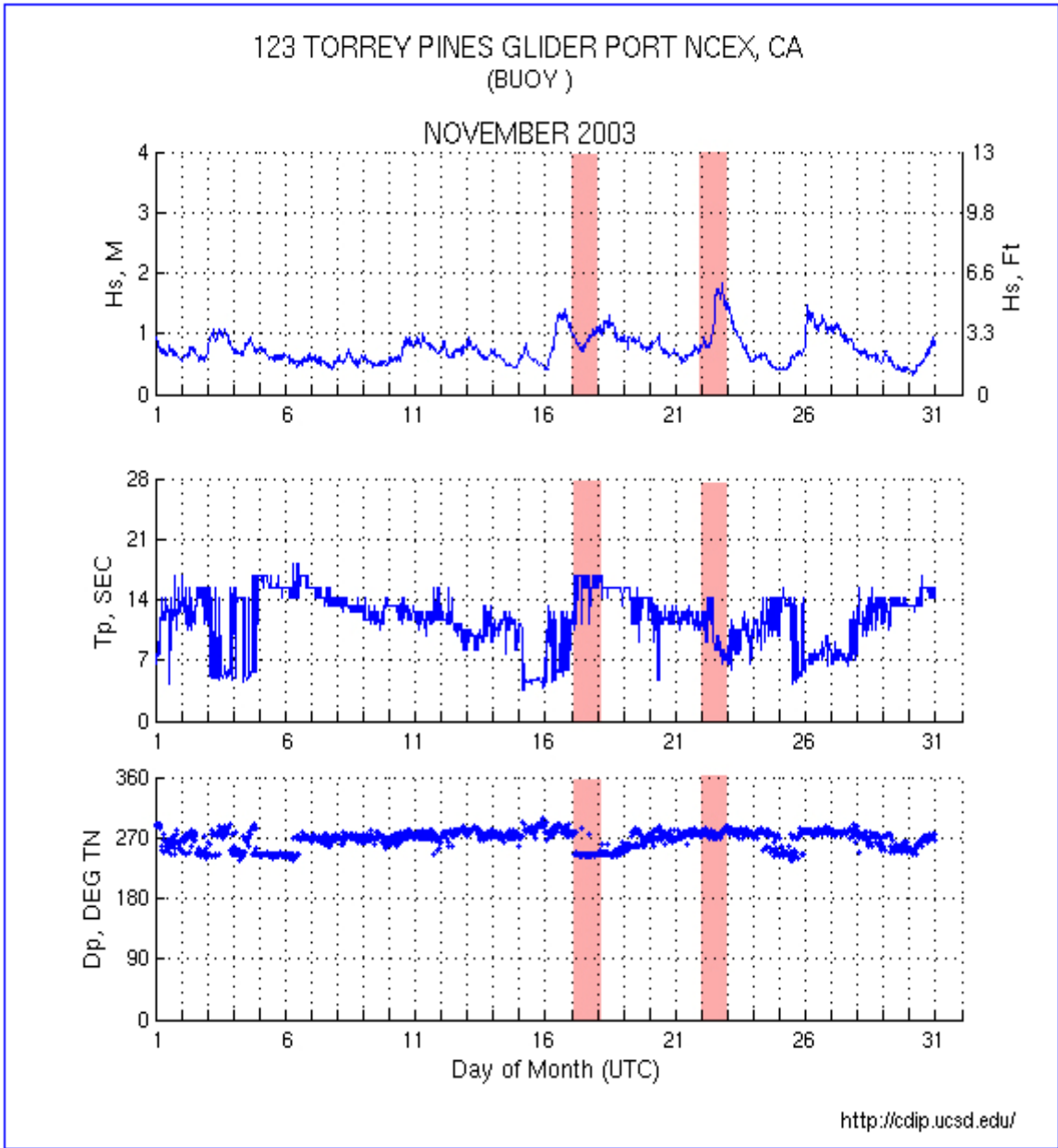


Figure 17. November 2003 wave statistics (same format as Figure 16).

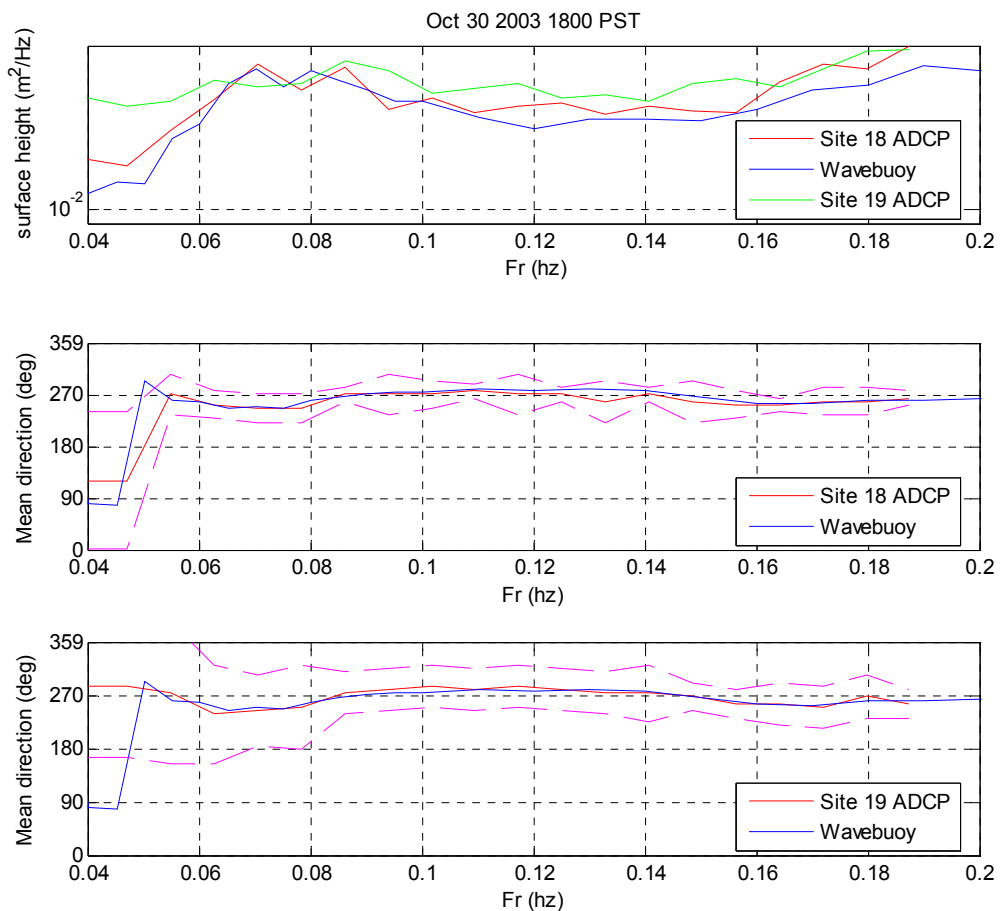


Figure 18. Case I ADCP and wave buoy comparisons. From top to bottom are shown the surface height spectrum, the mean direction for site 18 and mean direction for site 19. The dashed lines in the lower two panels indicate the mean direction  $\bar{\theta} \pm$  the directional spread  $\sigma$ .

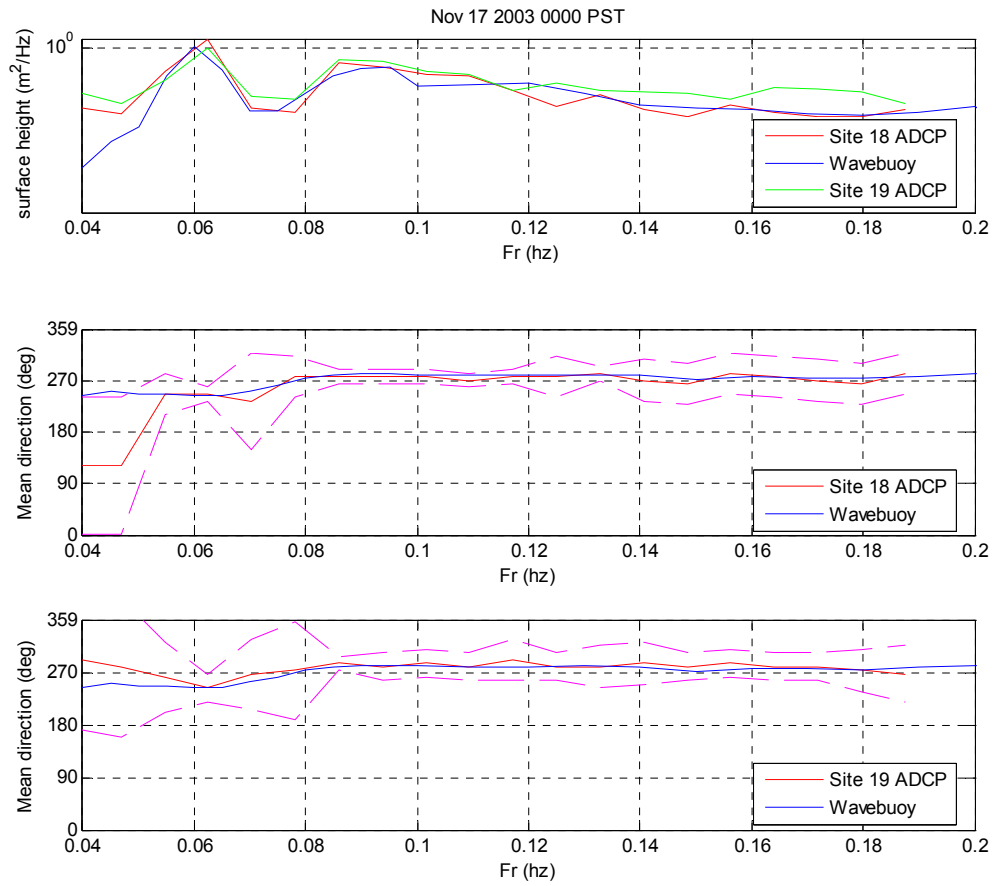


Figure 19. Case II ADCP and wave buoy comparisons (same format as Figure 18).

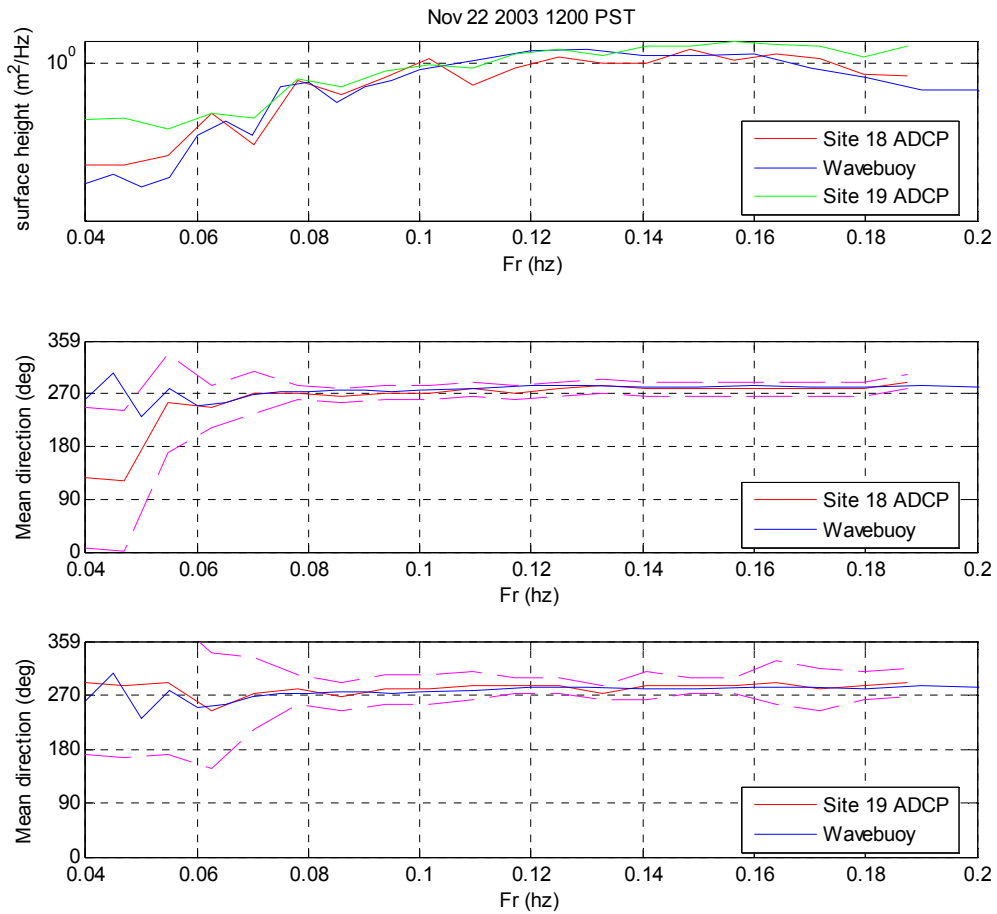


Figure 20. Case III ADCP and wave buoy comparisons (same format as Figure 18).

## VI. CONCLUSIONS

The Acoustic Doppler Current Profiler (ADCP) is the most widely used oceanographic instrument. This thesis examines the ADCP's ability to measure ocean waves in the nearshore environment. While previous studies have verified the ADCP's ability to measure surface wave height and mean direction, questions remained about the basic accuracy of the intrinsic ADCP velocity measurements sampled at a high rate. The goal of this thesis was to evaluate the performance of ADCP wave measurements in a realistic coastal environment.

During NCEX 2003, two Teledyne Workhorse Sentinel ADCP's were deployed near Scripps Canyon. The large data sets provided by the experiment were analyzed to determine the quality of the basic velocity measurements over a wide range of conditions and evaluate the reliability of wave height and direction spectra extracted from these data. Initial screening of the velocity time series data revealed that not all the data was readily usable and contained numerous dropouts which needed to be corrected. Some time series contained significant blocks of bad data that had to be discarded. Many data sets that contained isolated dropouts could be corrected by interpolating the dropouts through the cubic spline method.

The ADCP data quality was then verified through beam comparisons, examination of the high frequency spectral levels, and comparisons with pressure measurements using the linear wave theory transfer functions. Since the ADCP measures the same velocity variance in opposing beams, the data contain redundant information that can be used as a

consistency check. This check revealed that the lowest depth cells suffer from bottom interference. Another performance check of the ADCP used a pressure-velocity transfer function to relate the sum of the ADCP velocity spectra to the directly measured pressure spectrum. These revealed that the ADCP's velocity measurements are accurate in higher energy conditions and the upper water column. In low energy conditions and deeper in the water column, significant discrepancies were observed that are caused by a low signal to noise ratio.

Finally, linear wave theory transfer functions were used to extract surface height and direction spectra from the ADCP velocity measurements. These estimates were then compared to data from a Datawell Waverider buoy that was located between the two ADCP's. Three case studies were selected for comparisons which revealed that the shallower ADCP instrument performed better than the deeper instrument in measuring the sea surface height spectra. As expected for the observed swell conditions, the directional distributions of wave energy were narrow with a dominant westerly condition. Despite the relatively high noise levels, the mean wave directions measured by both ADCP's are in excellent agreement with the buoy data.

Overall the ADCP appears to be a viable instrument for routine wave measurements. While the ADCP may not be the panacea for detailed ocean wave measurements, its compact size, wide availability, and affordability provide the U.S. Navy with another tool to supplement its wave models. These advantages make the ADCP an ideal instrument to mount on AUVs which can be used to silently gather wave information in a hostile nearshore environment. Future

studies of the ADCP should be directed toward this application, in order to determine its effectiveness while deployed.

THIS PAGE INTENTIONALLY LEFT BLANK

## LIST OF REFERENCES

- Allendar, J., Audunson, S.F. Barstow, S. Bjerken, H. Krogstad, P. Steinbakke, L. Vartadal, L. Borgman, and C. Graham. The Wadic Project: A comprehensive field evaluation of directional wave instrumentation, *Ocean Eng.*, 16, 505-536, 1989.
- Beal, R., Directional Ocean Wave Spectra, *The John Hopkins Studies in Earth and Space Sciences*, 1-29, 1991.
- Bowden, K.F., and R.A. White. Measurements of the orbital velocities of sea waves and their use in determining the directional spectrum. *Geophys. J. R. Astron. Soc.*, 12, 33-54, 1966.
- Davis, R.E., and L.A. Regier. Methods for estimating directional wave spectra from multi-element arrays. *J. Mar Res.*, 35(3), 453-477, 1977.
- Guza, R.T., M.C. Clifton, and F. Rezvani. Field intercomparisons of electromagnetic current meters, *J. Geophys. Res.*, 93, 9302-9314, 1988.
- Herbers, T.H.C., R.L. Lowe, R.T. Guza. field verification of acoustic doppler surface gravity wave measurements, *J. of Geo. Res.* Vol. 96 No. C9, 17,023-17,035, 1991.
- Herbers, T.H.C., R.T. Guza. Estimation of directional wave spectra from multicomponent observations, *Journal of Physical Oceanography*, Vol. 20 NO., 1703-1723, 1990.
- Krogstad, H.E., R.L. Gordon and M.C. Miller. High resolution directional wave spectra from horizontally mounted acoustic Doppler current meters, *J. Atmos. Oceanic Technology*, 5, 340-352, 1988.
- Longuet-Higgins, M.S., D.E. Cartwright, and N. D. Smith. Observations of the directional spectrum of sea waves using the motions of a floating buoy. *Proc. Conf. Ocean Wave Spectra*, Prentice Hall, 111-132, 1963.
- Magne, R., K.A. Belibassakis, T.H.C. Herbers, Fabrice Ardhuin, W.C. O'Reilly, and V. Rey. Evolution of surface gravity waves over a submarine canyon. *J. Geophys. Res.*, in press, 2006.

Pawka, S.S. Island shadows in wave directional spectra. *J. Geophys. Res.*, 88(C4), 2579-2591, 1983

Peak, S.D. Wave Refraction over complex nearshore bathymetry, Master's Thesis, Naval Postgraduate School, Monterey California, 2004.

Pinkel, R., and J.A. Smith. Open ocean surface wave measurements using Doppler sonar, *J. Geophys. Res.*, 92, 12,967-12,973, 1987.

RD Instruments Waves Primer: Wave measurements and the RDI ADCP waves arrays technique, Retrieved October 2006, [http://www.rdinstruments.com/pdfs/waves\\_primer\\_0504.pdf](http://www.rdinstruments.com/pdfs/waves_primer_0504.pdf).

RD Instruments, Principles of Operation: A Practical Primer, 951-6069-00 Manual, Primer. RD Instruments, San Diego.

Smith, J. A., Doppler sonar and surface waves: Range and resolution, *J. Atmos. Oceanic Technology*, 6, 680-696, 1989.

Strong, B., B. Brumley, E.A. Terray, G.W. Stone, The performance of ADCP-Derived directional wave spectra and comparison with other independent measurements, RD Instruments, San Diego, 2000. Retrieved October 2006, <http://www.rdinstruments.com/pdfs/WavesBRO2000.pdf>.

Thornton, E.B. and R.F. Krapohl. Water particle velocities measured under ocean waves. *J. Geophys. Res.*, 79 (6), 847-852, 1974.

## INITIAL DISTRIBUTION LIST

1. Defense Technical Information Center  
Ft. Belvoir, Virginia
2. Dudley Knox Library  
Naval Postgraduate School  
Monterey, California
3. Professor Mary L. Batteen  
Department of Oceanography  
Naval Postgraduate School  
Monterey, California
4. Professor T.H.C. Herbers  
Department of Oceanography  
Naval Postgraduate School  
Monterey, California
5. Professor E.B. Thornton  
Department of Oceanography  
Naval Postgraduate School  
Monterey, California
6. Mr. Paul Jessen  
Department of Oceanography  
Naval Postgraduate  
Monterey, California